Main Manuscript and Supporting information for

CyAbrB2 is a nucleoid-associated protein in *Synechocystis* controlling hydrogenase expression during fermentation

Ryo Kariyazono[1] and Takashi Osanai[1]*

[1]School of Agriculture, Meiji University

*Takashi Osanai

Postal address: 1-1-1 Higashimita, Tama-ku, Kawasaki, Kanagawa 214-8571, Japan

Telephone/Fax: +81-44-934-7103

Email: tosanai@meiji.ac.jp

Author Contributions: RK and TO designed the study; RK performed the study; RK analyzed the data; RK and TO wrote the paper

Competing Interest Statement: The authors declare no conflict of interest.

Classification:

Major: Biological sciences

Minor: Plant Biology

Keywords: cyanobacteria, transcription, microoxic response, hydrogenase, nucleoid-associated protein, sigma factor

This PDF file includes:

Main Text

Figures 1 to 8

Table 1

Figures S1 to S10

Tables S1 to S4

Abstract

The *hox* operon in *Synechocystis* sp. PCC 6803, encoding bidirectional hydrogenase responsible for H_2 production, is transcriptionally upregulated under microoxic conditions. Although several regulators for *hox* transcription have been identified, their dynamics and higher-order DNA structure of *hox* region in microoxic conditions remain elusive. We focused on key regulators for the *hox* operon: cyAbrB2, a conserved regulator in cyanobacteria, and SigE, an alternative sigma factor. Chromatin immunoprecipitation-sequencing revealed that cyAbrB2 binds to the *hox* promoter region under aerobic conditions, with its binding being flattened in microoxic conditions. Concurrently, SigE exhibited increased localization to the *hox* promoter under microoxic conditions. Genome-wide analysis revealed that cyAbrB2 binds broadly to AT-rich genome regions and represses gene expression. Moreover, we demonstrated the physical interactions of the *hox* promoter region with its distal genomic loci. Both the transition to microoxic conditions and the absence of cyAbrB2 influenced the chromosomal interaction. From these results, we propose that cyAbrB2 is a cyanobacterial nucleoid-associated protein (NAP), modulating chromosomal conformation, which blocks RNA polymerase from the *hox* promoter in aerobic conditions. We further infer that cyAbrB2, with altered localization pattern upon microoxic conditions, modifies chromosomal conformation in microoxic conditions, which allows SigE-containing RNA polymerase to access the *hox* promoter. The coordinated actions of this NAP and the alternative sigma factor are crucial for the proper *hox* expression in microoxic conditions. Our results highlight the impact of cyanobacterial

46 chromosome conformation and NAPs on transcription, which have been insufficiently investigated.

47

48

49 **Introduction**

50 Cyanobacteria perform fermentation, using glycolytic products as electron acceptors. (1). Cyanobacteria

51 have multiple fermentation pathways according to the environment. For example, the freshwater living

52 cyanobacterium *Synechocystis* sp. PCC 6803 (hereafter referred to as *Synechocystis*) produces acetate,

53 lactate, dicarboxylic acids, and hydrogen (1, 2).

54 Hydrogen is generated in quantities comparable to lactate and dicarboxylic acids as the result of electron

55 acceptance in the dark microoxic condition (3, 4). Bidirectional hydrogenase is a key enzyme for H_2

56 production from protons (5) and is commonly found in cyanobacteria (6). Cyanobacterial hydrogenase

57 comprises five subunits (HoxEFUHY) containing nickel and Fe-S clusters (7). This enzyme can utilize

58 NADH, reduced ferredoxin, and flavodoxin as substrates (8). Hydrogenase mainly receives reduced

59 ferredoxin from pyruvate-ferredoxin oxidoreductase (PFOR) in the microoxic condition (8, 9).

60 Although hydrogenase and PFOR are O_2 sensitive, they can work under aerobic conditions (10–12).

61 Therefore, uncontrolled expression of *hox* operon and *nifJ* (coding gene of PFOR) may hamper metabolism

62 under photosynthetic conditions. Furthermore, genetic manipulations on *Synechocystis* have demonstrated

63 that modulating the expression of certain enzymes including hydrogenase can alter fermentative metabolic

64 flow (3, 4, 13). This provides evidence that transcription regulates the fermentative pathway. Thus,
65 transcriptional regulation in response to the environment is essential for optimal energy cost performance.
66 Promoter recognition by RNA polymerases is an essential step in transcriptional regulation. Sigma factors,
67 subunits of RNA polymerase, recognize core promoter sequences. Transcription factors can also bind to
68 promoter regions to suppress or promote RNA polymerase transcription. As well as recruitment or blocking
69 of RNA polymerase, some transcriptional factors, known as Nucleoid-associated proteins (NAPs),
70 modulate chromosomal conformation to regulate transcription (14). NAPs are common in bacteria, but
71 cyanobacterial NAPs remain unidentified, and higher-order DNA structure in cyanobacteria is yet to be
72 shown. A recent study suggested that the manipulation of chromosomal supercoiling impacts transcriptional
73 properties in cyanobacteria (15). There is room for consideration of NAPs modulating chromosomal
74 conformation and regulating expression in cyanobacteria.
75 In *Synechosysits*, the coding genes of HoxEFUHY form a single operon (sll1220–1226), while PFOR is
76 encoded in the *nifJ* (sll0741) gene. Both *hox* and *nifJ* operons are highly expressed under microoxic
77 conditions (16). Genetic analysis has revealed that multiple global transcriptional regulators control *hox*
78 and *nifJ* expression. Sigma factor SigE (Sll1689) promotes the expression of *hox* and *nifJ* operons (17, 18),
79 while transcription factor cyAbrB2 (Sll0822) represses them (19, 20). Positive regulators for the *hox* operon
80 include LexA (Sll1626) and cyAbrB1 (Sll0359) (21–23).
81 SigE, an alternative sigma factor, controls the expression of genes involved in glycogen catabolism and

82 glycolysis, as well as PFOR/*nifJ* and hydrogenase (17). SigE shows a high amino acid sequence similarity
83 with the primary sigma factor SigA, which is responsible for transcribing housekeeping and photosynthetic
84 genes (24). A ChIP-seq study revealed that, while most SigE-binding sites are the same as SigA, SigE
85 exclusively occupies the promoters of glycogen catabolism and glycolysis (25).

86 CyAbrB2 and its homolog cyAbrB1 are transcription factors highly conserved in cyanobacteria. For
87 example, cyAbrB homologs in *Anabaena* sp. PCC7120 is involved in heterocyst formation (26). CyAbrB2
88 in *Synechocystis* regulates the expression of several genes involved in carbon metabolism, nitrogen
89 metabolism, and cell division (20, 27, 28). CyAbrB2 binds to the *hox* promoter *in vitro* and represses its
90 expression *in vivo* (19). CyAbrB1, an essential gene, physically interacts with the cyAbrB2 protein (29)
91 and binds the *hox* promotor region *in vitro* to promote its expression (21).

92 To explore the dynamics of those transcription factors governing the expression of *hox* operon, we
93 conducted a time-course analysis of the transcriptome and ChIP-seq of SigE and cyAbrB2. Our ChIP-seq
94 and transcriptome analysis showed the NAPs-like nature of cyAbrB2, which prompted us to conduct a
95 chromosomal conformation capture assay. 3C analysis explored the physical interaction between the *hox*
96 promoter region and its downstream and upstream genomic region in the aerobic condition, and some loci
97 changed interaction frequency upon entry to the microoxic condition. Furthermore, some interactions in
98 the Δ*cyabrB2* mutant were different from those of the wildtype. From those experiments, we propose that
99 cyAbrB2 modulates chromosomal conformation like NAPs, allowing access to the SigE-containing RNA

100 polymerase complex on the *hox* promoter, by which the *hox* operon achieves distinct expression dynamics.

101 Chromosomal conformation of bacteria is a growing area of interest, and the findings of this study have

102 brought insight into the transcriptional regulation of cyanobacteria.

103 **Results**

104 **Transcriptomes on entry to dark microoxic conditions**

105 To understand transcriptional regulation under microoxic conditions, we conducted a time-course

106 transcriptome capturing light aerobic and dark microoxic conditions at 1-, 2-, and 4-hours time points

107 (Figure 1A). Gene set enrichment analysis based on KEGG pathway revealed that many biological

108 pathways, including photosynthesis and respiration (oxidative phosphorylation), were downregulated by

109 the transition to dark microoxic conditions from light aerobic conditions (Figure 1B). Upregulated

110 pathways included butanoate metabolism and two-component systems. The enrichment in the butanoate

111 metabolism pathway indicates the upregulation of genes involved in carbohydrate metabolism. We further

112 classified genes according to their expression dynamics. Within 1 hour of switching from aerobic to

113 microoxic conditions, the expression levels of 508 genes increased more than 2-fold. Furthermore, genes

114 with increased expression levels were classified into four groups based on the time course (Figures 1C and

115 S1). Of the 508 genes, 28 were termed “transiently upregulated genes” due to their decreased expression

116 upon the comparison of 1- and 4-hours incubation under microoxic conditions (log2 fold change < -0.5),

117 and 119 were termed “continuously upregulated genes.”, which continuously increased between 1- and 4-

118 hours incubation under microoxic conditions (log2-fold change > 0.5). Other than 508 genes 2-fold
119 upregulated within 1 hour, 28 genes showed more than 4-fold increment within 4 hours but not upregulated
120 within 1 hour. We combined those "Late upregulated genes" with 508 genes and referred to as "All
121 upregulated genes" in the subsequent analysis (Figure S1). Mapping the classified genes to central carbon
122 metabolism revealed that *nifJ* encoding PFOR and *hox* operon encoding a bidirectional hydrogenase
123 complex were transiently upregulated (Figure 1D and Table 1). RTqPCR verified the transient expression
124 of *hoxF*, *hoxH,* and *nifJ* (Figure S2).

125 **SigE and cyAbrB2 control the expression of transiently upregulated genes**

126 The functional correlation between hydrogenase and PFOR, encoded by the *hox* operon and *nifJ,* suggests
127 that transient upregulation has physiological significance. We focused on transiently upregulated genes and
128 attempted to reveal the regulatory mechanism underlying transient upregulation. While SigE promotes the
129 expression of *hox* and *nifJ*, cyAbrB2 represses them (17, 19, 20). We confirmed that the deletion of *sigE*
130 and *cyabrb2* (Δ*sigE* and Δ*cyabrb2*, respectively) affected the expression of *hoxF*, *hoxH*, and *nifJ* by RT-
131 qPCR (Figure S1). Thus, we conducted a time-course transcriptome analysis of Δ*sigE* and Δ*cyabrb2* under
132 aerobic conditions and after 1- and 2-hours cultivation in dark microoxic conditions (Figures 2A and S3).
133 The transcriptome data confirmed that SigE and cyAbrB2 regulated *hox* operon expression (Figure 2B). At
134 each time point, we searched for differentially expressed genes (DEGs) between mutants and wildtype with
135 a more than 2-fold expression change and a false discovery rate (FDR) less than 0.05. We found that deleting

136 *sigE* or *cyabrb2* preferentially affected the expression of transiently upregulated genes, not limited to *hox*

137 and *nifJ* operons (Figures 2C and 2D). Interestingly, *cyabrb2* deletion resulted in the upregulated expression

138 of transient genes under aerobic conditions, in contrast to 1-hour cultivation under microoxic conditions

139 (Figure 2C).

140 **Genome-wide analysis of cyAbrB2, cyAbrB1, and SigE via ChIP-seq**

141 To decipher the regulatory mechanism of transiently upregulated genes, we must first comprehend the

142 fundamental features and functions of these transcriptional regulators. Therefore, a genome-wide survey of

143 cyAbrB2 and SigE occupation (Figure S4) combined with transcriptome data was done. Specifically, we

144 generated a *Synechocystis* strain in which cyAbrB2 was epitope-tagged and performed a ChIP-seq assay

145 under aerobic and microoxic conditions (Figure S4A). SigE-tagged strains previously constructed and

146 analyzed elsewhere were also employed (25). The primary sigma factor SigA was also analyzed to

147 determine SigE-specific binding. In addition to cyAbrB2, we tagged and analyzed cyAbrB1, which is the

148 interactor of cyAbrB2 and positively regulates the *hox* operon.

149 **CyAbrB2 binds to long tracts of the genomic region and suppresses genes in the binding region**

150 The ChIP-seq data showed that cyAbrB2 bound to long tracts of the genomic region with lower GC

151 content than the whole genome *Synechocystis* (Figures 3A and 3B). Vice versa, regions exhibiting lower

152 GC contents showed a greater binding signal of cyAbrB2 (Figure 3C). This correlation was not a systematic

153 bias of next-generation sequencing because the binding signals of SigE, SigA, and control showed no

154 negative correlation to GC contents (Figures S5A and S5B). The binding regions of cyAbrB2 called by
155 peak-caller covered 15.7% of the entire genome length. 805 of 3614 genes overlapped with cyAbrB2
156 binding regions, and almost half (399 of 805 genes) were entirely covered by cyAbrB2 binding regions.
157 The cyAbrB2 binding regions included 80 of 125 insertion sequence elements (Figure 3D). Comparison
158 with the transcriptome of Δ*cyabrB2* revealed that cyAbrB2 tended to suppress the genes overlapping with
159 its binding regions under aerobic conditions (Figures 3A and 3E). A survey of the genomic localization of
160 cyAbrB1 under aerobic conditions revealed that cyAbrB1 and cyAbrB2 shared similar binding patterns
161 (Figures 3A and S5C). Due to the essentiality of cyAbrB1, we did not perform transcriptome analysis on a
162 cyAbrB1-disrupted strain. Instead, we referred to the recent study performing transcriptome of cyAbrB1
163 knockdown strain, whose cyAbrB1 protein amount drops by half (30). Among 24 genes induced by
164 cyAbrB1 knockdown, 12 genes are differentially downregulated genes in *cyabrb2*Δ in our study (Figure
165 S5D).

166 **CyAbrB2 binds to transiently upregulated genes**

167 The binding regions of cyAbrB2 overlapped 17 of 28 transiently upregulated genes, showing significant
168 enrichment from all upregulated genes (Figure 4A). The transiently upregulated genes belong to 17
169 transcriptional units (TUs), according to the previous study(31), and cyAbrB2 tends to bind TUs with
170 transiently upregulated genes (Figure 4B). While cyAbrB2 covered the entire length of insertion sequences
171 and unknown proteins, its binding positions on other transient genes were diverse (Figure 4C). Specifically,

172 the *hox* and *nifJ* operons had two distinct binding regions located at the transcription start sites (TSSs) and

173 middle of operons, the *pntAB* operon had two binding regions in the middle and downstream of the operon,

174 and the *nrtABCD* operon had one binding region downstream of the operon (Figure 4C).

175 **Localization of cyAbrB2 became blurry under the microoxic condition**

176 When cells entered microoxic conditions, the relative ChIP-seq signals in the cyAbrB2 binding regions

177 slightly declined (Figures 5A and 5B). Notably, the total quantities of precipitated DNA by tagged cyAbrB2

178 did not decrease (Figure S6A), and qPCR confirmed that the cyAbrB2 binding signal increased in all

179 positions tested (Figure 5C). ChIP-seq data and ChIP-qPCR data indicate that the boundary between

180 cyAbrB2 binding region and cyAbrB2-free region became obscured when the cells entered microoxic

181 conditions due to increased binding of cyAbrB2 to both cyAbrB2 binding and cyAbrB2-free region. The

182 protein amount of cyAbrB2 was not altered on entry to the microoxic condition (Figure S6B). The cyAbrB2

183 binding signal around the transiently upregulated genes became less specific upon entry into microoxic

184 conditions, consistent with the general tendency (Figure 5B). The amount of DNA immunoprecipitated by

185 cyAbrB1 was also increased in the microoxic condition, and the protein amount was not increased (Figures

186 S6C and S6D).

187 **Sigma factors SigE and SigA are excluded from cyAbrB2 binding regions regardless of GC contents**

188 We searched for SigE and SigA binding sites under aerobic and microoxic conditions (Figures S7A and

189 S7B, left and right, respectively). The SigE and SigA peaks identified in this study predominantly covered

190 the previously identified peaks (Figure S7C), reproducing the previous study's conclusion (25); i.e., SigE
191 and the primary sigma factor SigA share localization on the promoters of housekeeping genes, but SigE
192 exclusively binds to the promoters of its dependent genes. SigE and SigA binding peaks were significantly
193 excluded from the cyAbrB2 binding regions (Figures 6A and 6B). SigE preferred the cyAbrB2-free region
194 in the aerobic condition more than SigA did (Odds ratios of SigE and SigA being in the cyAbrB2-free
195 region were 4.88 and 2.74, respectively). CyAbrB2 prefers AT-rich regions, but no correlation was found
196 between the GC content and binding signals of SigE and SigA (Figures S5A and S5B). Thus, SigA and
197 SigE are excluded from cyAbrB2 binding regions regardless of GC contents.

198 **Dynamics of sigma factors upon exposure to the microoxic condition**

199 When cells entered microoxic conditions, the binding signals of SigA and SigE were changed, although
200 most of their peaks observed under aerobic conditions were present under microoxic conditions (Figure
201 S7A). The preference of SigE for the cyAbrB2-free region was alleviated in the microoxic condition (Figure
202 6A). Next, we focused on sigma factor dynamics in transiently upregulated genes. SigE, but not SigA, binds
203 at the TSS of *pntAB* under aerobic and microoxic conditions (Figure 6C top). SigE binding summits were
204 not identified at the TSSs of the *hox* and *nifJ* operons under aerobic conditions. However, the SigE-specific
205 binding summit appeared at the TSS of *nifJ* when cells entered microoxic conditions (Figure 6C middle).
206 A bimodal peak of SigE was observed at the TSS of the *hox* operon in a microoxic-specific manner (Figure
207 6C bottom panel). The downstream side of the bimodal SigE peak coincides with the SigA peak and the

208 TSS of TU1715. Another side of the bimodal peak lacked SigA binding and was located at the TSS of the

209 *hox* operon (marked with an arrow in Figure 6C), although the peak caller failed to recognize it as a peak.

210 SigE binding without SigA on the promoters of *hox*, *nifj*, and *pntAB* is consistent with their SigE-dependent

211 expression (Figure 2B).

212 **Chromatin conformation around *hox* operon and *nifJ* operon**

213 We have shown that cyAbrB2 broadly binds to AT-rich genomic regions, including insertion element

214 sequences, and represses expression (Figure 3). This is functionally similar to the NAPs (14), which

215 makes us hypothesize that cyAbrB2 modulates chromosomal conformation. Therefore, we conducted the

216 chromatin conformation capture (3C) assay against wildtype and *cyabrb2*Δ strains at aerobic and

217 microoxic conditions. qPCR was performed with unidirectional primer sets, where the genomic fragment

218 containing *hox* operon and *nif* operon (hereinafter *hox* fragment and *nifJ* fragment, respectively) were

219 used as bait (Figure 7).

220 First, focusing on the aerobic condition of wildtype (Figure 7B, solid line), the *hox* fragment interacted

221 with its proximal downstream loci (loci (f) to (g)) and proximal upstream locus (locus (j)). The *hox*

222 fragment also interacts with the distal downstream locus (locus (c)). Meanwhile, the *nifJ* fragment shows

223 high interaction frequency with proximal upstream and downstream loci (Figure 7G, loci (i') and (j')),

224 and a distal downstream locus (locus (g')) showed higher interaction frequency with *nifJ* fragment than

225 proximal locus (h') did. The upstream regions of *nifJ* (loci (l') to (n') and (p')) showed comparable

226 frequency with locus (g').

227 **The chromatin conformation is changed in *cyabrb2*Δ in some loci**

228 Then we compared the chromatin conformation of wildtype and *cyabrb2*Δ. Although overall shapes of

229 graphs did not differ, some differences were observed in wildtype and *cyabrb2*Δ (Figures 7B and 7G);

230 interaction of locus (c) with *hox* region were slightly lower in *cyabrb2*Δ and interaction of loci (f') and

231 (g') with *nifJ* region were different in wildtype and *cyabrb2*Δ. Note that the interaction scores exhibit

232 considerable variability and we could not detect statistical significance at those loci.

233 **Changes of chromatin conformation upon microoxic condition**

234 When the cells entered the microoxic condition, proximal loci interacted more frequently (Figure 7D;

235 loci (f)-(h) and Figure 7I loci (j') and (k')). This tendency was more apparent in *cyabrb2*Δ (Figures 7E

236 and 7J). Furthermore, the interaction of *nifJ* upstream loci (l') – (n') increased in the microoxic condition

237 in *cyabrb2*Δ but not wildtype (Figures 7I and 7J). The locus (c) and locus (j) interacted less frequently

238 with *hox* fragment upon entry to the microoxic condition in the wildtype. While the interaction scores

239 exhibit considerable variability, the individual data over time demonstrate declining trends of the wildtype

240 at locus (c) and (j) (Figure S8). In Δ*cyabrb2*, by contrast, the interaction frequency of loci (c) and (j) was

241 unchanged in the aerobic and microoxic conditions (Figure 7E). The interaction frequency of locus (c) in

242 Δ*cyabrb2* was as low as that in the microoxic condition of wildtype, while that of locus (j) in Δ*cyabrb2*

243 was as high as that in the aerobic condition of wildtype (Figures 7B and 7C). In summary, 3C analysis

244 demonstrated cyAbrB2-dependent and independent dynamics of chromosomal conformation around the

245 *hox* and *nifJ* operon in response to the microoxic condition (Figure 8).

246 **Discussion**

247 **Physiological significance of transient upregulation of *hox* and *nifJ* operons**

248 As the transcriptional change can alter the metabolic flow, the transcriptional upregulation of fermentative

249 genes in response to the microoxic condition is expected to be adaptive for energy acquisition and the

250 maintenance of redox balance. Our time-course transcriptome showed upregulation of several genes

251 involved in catabolism upon exposure to the microoxic condition. The transient upregulation of *hox* and

252 *nifJ* operons is distinctive among them (Figure 1D).

253 One reason for transient upregulation is probably the resource constraints of inorganic cofactors.

254 Hydrogenase and PFOR (the product of *nifJ* gene) have iron-sulfur clusters, and hydrogenase requires

255 nickel for its activity (32, 33). Overexpression of the *hox* operon should be futile under physiological

256 conditions without an adequate nickel supply (34).

257 Another significance for transient upregulation may be the reusability of fermentative products. Hydrogen,

258 lactate, and dicarboxylic acids can be reused as the source of reducing power when cells return to aerobic

259 conditions (12, 35, 36). The substrate proton is abundant, but hydrogen is diffusive and difficult to store.

260 Therefore, hydrogenase may favor fermentation initiation, and the reductive branch of TCA-producing

261 dicarboxylic acids may become active subsequently. In fact, *citH*/*mdh* (sll0891) encoding a key enzyme of

262 the reductive branch of TCA was classified as continuously upregulated genes in this study (Figures 1C and

263 1D).

264 **Mechanisms for transient expression mediated by SigE and cyAbrB2**

265 SigE and cyAbrB2 can independently contribute to the transient transcriptional upregulation. This is

266 evident as the single mutants, Δ*sigE* or Δ*cyabrb2*, maintained transient expression of *hoxF* and *nifJ* (Figure

267 S2). We first discuss cyAbrB2 as the potential NAPs, and then the mechanism of transient upregulation

268 mediated by cyAbrB2 and SigE will be discussed.

269 **cyAbrB2 is a novel nucleoid-associated protein of cyanobacteria**

270 We have shown that cyAbrB2 broadly binds to AT-rich genomic regions, including IS elements (Figure

271 3). This is functionally similar to the histone-like nucleoid protein H-NS family; including H-NS in

272 *Enterobacteriaceae* (37, 38)*, and* Lsr2 in *Mycobacteria* (39). Like H-NS and Lsr2, cyAbrB2 may defend

273 against exogenous DNA elements, which often have different GC content. Interestingly, Lsr2 controls genes

274 responding to hypoxia, showing a functional analogy with cyAbrB2 (40).

275 **The biochemistry of cyAbrB2 will shed light on the regulation of chromatin conformation in the**

276 **future**

277 H-NS proteins often cause bound DNA to bend, stiffen, and/or bridge (14). DNA-bound cyAbrB2 is

278 expected to oligomerize, based on the long tract of cyAbrB2 binding region in our ChIP-seq data. However,

279 no biochemical data mentioned the DNA deforming function or oligomerization of cyAbrB2 in the previous

280 studies, and preference for AT-rich DNA is not fully demonstrated in vitro (19, 27, 41). Moreover, our 3C
281 data did not support bridging at least in *hox* region and *nifJ* region, as the high interaction locus and
282 cyAbrB2 binding region did not seem to correlate (Figure 7). Therefore, direct observation of the DNA-
283 cyAbrB2 complex by atomic force microscopy is the solution in the future.

284 Not only DNA structural change but also the effect of the post-translational modification can be
285 investigated by biochemistry. The previous studies report that cyAbrB2 is subject to phosphorylation and
286 glutathionylation (42, 43), and pH and redox state alters cyAbrB1's affinity to DNA (41). Those
287 modifications might respond to environmental changes and be involved in transient expression. Overall,
288 the biochemistry integrating assay conditions (PTM, buffer condition, and cooperation with cyAbrB1) and
289 output (DNA binding, oligomerization, and DNA structure) will deepen the understanding of cyAbrB2 as
290 cyanobacterial NAPs.

291 **Cooperative and antagonistic function of cyAbrB1 and cyAbrB2**

292 CyAbrB1, the homolog of cyAbrB2, may cooperatively work, as cyAbrB1 directly interacts with cyAbrB2
293 (29), their distribution is similar, and they partially share their target genes for suppression (Figures 3A S5C
294 and S5D). The possibility of cooperation would be examined by the electrophoretic mobility shift assay of
295 cyAbrB1 and cyAbrB2 as a complex. Despite their similar repressive function, cyAbrB1 and cyAbrB2
296 regulate *hox* expression in opposite directions, and their mechanism remains elusive. The stoichiometry of
297 cyAbrB1 and cyAbrB2 bound to DNA fluctuates in response to the environmental changes (28), but there

298 was no difference in the behavior of cyAbrB1 and cyAbrB2 around the *hox* region on entry to the microoxic

299 condition.

300 **Localization pattern and function of cyAbrB2**

301 Herein, we classified three types of binding patterns for cyAbrB2. The first is that cyAbrB2 binds a long

302 DNA tract covering the entire gene or operon, represented by the insertion sequence elements. CyAbrB2

303 suppresses expression in this pattern (Figure 3E). In the second pattern, cyAbrB2 binds on promoter regions,

304 such as *hox* operon and *nifJ*. The binding on those promoters fluctuates in response to environmental

305 changes, thus regulating expression. This pattern also applies to the promoter of *sbtA* (Na^+/HCO_3^-

306 symporter), where cyAbrB2 is bound in a CO_2 concentration-dependent manner (28). The last one is

307 cyAbrB2 binding in the middle or downstream of operons. The middle of *hox*, *pntAB*, and *nifJ* operons and

308 the downstream of *nrt* operon are the cases (Figure 4C). Our data show that genes in the same operon

309 separated by the cyAbrB2 binding region behave differently. In particular, *pntB* is classified as the

310 transiently upregulated gene, while *pntA* is not, despite being in the same operon. This might be explained

311 by the recent study which reported that cyAbrB2 affects the stability of mRNA transcribed from its binding

312 gene (41). The cyAbrB2-mediated stability of mRNA may also account for the decrease in transcript from

313 transient upregulated genes at 4 hours of cultivation. Hereafter, we will focus on the mechanism of the

314 second pattern, regulation by cyAbrB2 on the promoter.

315 **Insight into the regulation of *hox* and *nifJ* operon by cyAbrB2**

316 Genome-wide analysis indicates that the cyAbrB2-bound region blocks SigE and SigA (Figures 6A and
317 6B). This is presumably because sigma factors recognize the promoter as a large complex of RNA
318 polymerase. CyAbrB2 binds to the *hox and nifJ* promoter region and may inhibit access to RNA polymerase
319 complex under aerobic conditions. When cells entered microoxic conditions, the boundaries of the cyAbrB2
320 binding region and cyAbrB2-free region became obscure (Figure 5), and SigE binding peaks on those
321 promoters became prominent (Figure 6C). Notably, cyAbrB2 ChIP efficiency at the *hox* promoter is higher
322 in the microoxic condition than in the aerobic condition (Figure 5). Hence, while the exclusion by cyAbrB2
323 occupancy on promoter inhibits containing RNA polymerase in the aerobic condition, it is also plausible
324 that chromosomal conformation change governed by cyAbrB2 provides SigE-containing RNA polymerase
325 with access to the promoter region (Figure 8). Our 3C result demonstrated that cyAbrB2 influences the
326 chromosomal conformation of *hox* and *nifJ* region to some extent (Figure 7).

327 A recent study demonstrated that manipulating the expression of topoisomerase, which influences
328 chromosomal conformational change through supercoiling, affects transcriptional properties in
329 cyanobacteria (15). Moreover, Song et al. pointed out that DNA looping may inhibit transcription in
330 cyanobacteria (41) because artificial DNA looping by the LacI repressor of *E. coli* can repress
331 cyanobacterial transcription (44). Thus, we infer conformation change detected by the present 3C
332 experiment regulates expression of *hox* operon.

333 **Generality for chromosomal conformation in cyanobacteria**

334 Our 3C analysis revealed that local chromosomal conformation changes upon entry to the microoxic
335 conditions (Figure 8). As cyAbrB2 occupies about 15% of the entire genome and globally regulates gene
336 expression, cyAbrB2 likely governs the whole chromosomal conformation. Furthermore, the
337 conformational changes by deletion of cyAbrB2 were limited, suggesting there are potential NAPs in
338 cyanobacteria yet to be characterized. It is speculated that conformational change of the entire chromosome
339 occurs to deal with many environmental stresses.

340 **The sigE-mediated mechanism for the transient expression**

341 One possible SigE-mediated mechanism for transient expression is the post-transcriptional activation and
342 degradation of SigE in the dark; i.e., SigE is sequestered by anti-sigma factor under light conditions and
343 released under dark (45), enabling acute transcription of *hox* operon and *nifJ*. Transcripts of *sigE* were
344 continuously downregulated in our time-course transcriptome, while *sigB* (sll0306) and *sigC* (sll0184) were
345 classified as continuous upregulated genes (Supplemental Table S1). It is possible that upregulated SigB
346 and SigC outcompete SigE in prolonged incubation under microoxic conditions. Finally, SigE is degraded
347 under dark within 24 hours (46).

348 Another reason for the microoxic specific expression may exist in the sequence of the *hox* promoter. We
349 previously determined the consensus sequence of -10 element for SigE regulon in the aerobic condition as
350 "TANNNT," where N is rich in cytosine (25). The -10 sequence of the *hox* promoter "TAACAA" (23)
351 deviates from the consensus, and no hexamer precisely fitting the consensus is found in the *nifJ* promoter.

352 This deviation can inhibit SigE from binding during aerobic conditions, aside from cyAbrB2-mediated
353 inhibition. Under the microoxic condition, transcription factors LexA (23) and Rre34 (16) may aid SigE
354 binding to the promoter of *hox* and *nifJ*, respectively.

355 Moreover, SigE seems susceptible to the blocking from cyAbrB2 during the aerobic condition compared
356 with SigA. This is supported by the odds ratio of SigE being in the cyAbrB2-free region was higher than
357 that of SigA in the aerobic condition (Figures 6A and 6B). The higher exclusion pressure of cyAbrB2 on
358 SigE may contribute to sharpening the transcriptional response of hox and nifJ on entry to microoxic
359 conditions. Overall, multiple environmental signals are integrated into the *hox* and *nifJ* promoter through
360 the cyAbrB2 and SigE dynamics.

361

362 **Materials and Methods**

363 **Bacterial strains and plasmids**

364 The glucose-tolerant strain of *Synechocystis* sp. PCC 6803 (47) was used as a wildtype strain in this study.
365 The *sigE* (sll1689)-disrupted strain (G50), SigE FLAG-tagged strain, and SigA FLAG-tagged strain were
366 constructed in a previous study (17, 25). Disruption and epitope-tagging of *cyabrb1*(sll0359) and
367 *cyabrb2*(sll0822) were performed by homologous double recombination between the genome and PCR
368 fragment (47). The resulting transformants were selected using three passages on BG-11 plates containing
369 5 μg/mL kanamycin. Genomic PCR was used to confirm the insertion of epitope tag fragments and gene

370 disruption (Figure S9). Supplemental Tables S2, S3, and S4 contain the cyanobacterial strains,
371 oligonucleotides, and plasmids used in this study.

372 **Aerobic and microoxic culture conditions**

373 For aerobic conditions, cells were harvested after 24 hours cultivation in HEPES-buffered BG-11_0 medium
374 (48), which was buffered with 20 mM HEPES-KOH (pH 7.8) containing 5 mM NH_4Cl under continuous
375 exposure to white light (40 μmol $m^{-2}s^{-1}$) and bubbled with air containing 1% CO_2 (final OD_{730} = 1.4–1.8).
376 For the dark microoxic culture, the aerobic culture cell was concentrated to an OD_{730} of 20 with the
377 centrifuge and resuspended in the culture medium. The concentrated cultures were poured into vials,
378 bubbled with N_2 gas, and sealed. The sealed vials were shaded and shaken at 30˚C for the described times.

379 **Antibodies and immunoblotting**

380 Sample preparation for immunoblotting was performed as previously described (25), and FLAG-tagged
381 proteins were detected by alkaline-phosphatase-conjugated anti-FLAG IgG (A9469, Sigma Aldrich, St.
382 Louis, MO) and 1-Step NBT/BCIP substrate solution (Thermo Fisher Scientific, Waltham, MA).

383 **RNA isolation**

384 Total RNA was isolated with ISOGEN (Nippon gene, Tokyo, Japan) following the manufacturer's
385 instructions and stored at −80˚C until use. The extracted RNA was treated with TURBO DNase (Thermo
386 Fisher Scientific) for 1 hour at 37˚C to remove any genomic DNA contamination. We confirmed that the
387 A260/A280 of the extracted RNA was >1.9 by NanoDrop Lite (Thermo Fisher Scientific). We prepared

388 triplicates for each timepoint for the RNA-seq library. RT-qPCR was performed as described elsewhere
389 (46).

390 **ChIP assay**

391 Two biological replicates were used for each ChIP-seq experiment, and one untagged control ChIP was
392 performed. ChIP and qPCR analyses were performed using the modified version of a previous method (25).
393 FLAG-tagged proteins were immunoprecipitated with FLAG-M2 antibody (F1804 Sigma-Aldrich)
394 conjugated to protein G dynabeads (Thermo Fisher Scientific).

395 **Library preparation and next-generation sequencing**

396 For the ChIP-seq library, input and immunoprecipitated DNA were prepared into multiplexed libraries
397 using NEBNext Ultra II DNA Library Prep Kit for Illumina (New England Biolabs, Ipswich, MA). For the
398 RNA-seq library, isolated RNA samples were deprived of ribosomal RNA with Illumina Ribo-Zero Plus
399 rRNA Depletion Kit (Illumina, San Diego, CA) and processed into a cDNA library for Illumina with the
400 NEBNext Ultra II Directional RNA Library Prep Kit for Illumina (New England Biolabs). Dual-index
401 primers were conjugated with NEBNext Multiplex Oligos for Illumina (Set1, New England Biolabs). We
402 pooled all libraries, and the multiplexed libraries were dispatched to Macrogen Japan Inc. and subjected to
403 paired-end sequencing with HiSeqX. Adapter trimming and quality filtering of raw sequence reads were
404 conducted with fastp (ver. 0.21.0) (49) under default conditions. The paired-end sequences were mapped
405 onto the *Synechocystis* genome (ASM972v1) using Bowtie2 (50) (ver. 2.4.5 paired-end). Supplementary

406 Table S5 contains the read counts that passed via fastp quality control and were mapped by Bowtie2.

407 **RNA-seq analysis**

408 Mapped reads were counted by HT-seq count (ver. 2.0.2) (51) for the GFF file of ASM972v1, with the

409 reverse-strandedness option. EdgeR package (ver. 3.40.1) (52) was used to perform the differential

410 expression analysis. Fold changes in expression and FDR were used for gene classification. Supplemental

411 Table S6-S8 contains fold change in gene expression calculated by edgeR.

412 **Genome-wide analyses**

413 Peaks were called using the MACS3 program (ver. 3.0.0b1) (53). For paired-end reads for SigE, SigA,

414 and untagged control ChIP, narrow peaks were called with <1e−20 of the q-value cut-off and "--call-

415 summits" options. The peak summits from two replicates and the untagged control were merged if summits

416 were located within 40 bp of each other. Peak summits identified in both replicates but not in the control,

417 were considered for further analysis. The midpoint of the peak summits for the two merged replicates was

418 further analyzed.

419 Broad peak calling methods were applied to paired-end reads for cyAbrB2, cyAbrB1, and untagged

420 control ChIP using the "–broad" option, with a q-value cut-off of < 0.05 and a q-value broad cut-off of <

421 0.05. The intersection of broad peaks from two replicates, excluding those called by the control, was used

422 in subsequent analyses.

423 The positions of the TSS, including internal start sites, were obtained as reported by (31). The read count,

424 merging, and intersection of the binding region were calculated using BEDTools (ver. 2.30.0) (54).
425 Supplemental Tables S9–S15 contain SigA and SigE peaks and the broad binding regions of cyAbrB2 and
426 cyAbrB1, respectively.
427 Binding signals in every 100 bp bin for scatter plots were calculated as (IP read counts within 100 bp
428 window) / (input read counts within 100 bp window) * (total input read counts/total IP read counts). GC
429 contents were calculated within 500 bp in 100 bp sliding windows by seqkit (ver. 2.3.0) (55).
430 **Genome extraction, digestion, and ligation for 3C assay**
431 A 3C assay was conducted based on the previous prokaryotic Hi-C experiment (56, 57), with certain steps
432 modified. To begin, *Synechocystis* were fixed with 2.5% formaldehyde for 15 minutes at room temperature.
433 Fixation was terminated by adding a final concentration of 0.5M of glycine, and cells were stored at -80˚C
434 until use. Fixed cells were disrupted using glass beads and shake master NEO (Bio Medical Science, Tokyo,
435 Japan), following the previous study's instructions for preparing cell lysate for ChIP. The lysates were
436 incubated with buffer containing 1mM Tris-HCl (pH7.5), 0.1mM EDTA, and 0.5% SDS for 10min at room
437 temperature, and 1% Triton X-100 quenched SDS. Genomes in the cell lysate were digested by 600U/mL
438 of HindIII (Takara Bio, Shiga, Japan) for 4 hours at 37˚C, and RNA in the lysate was simultaneously
439 removed by 50 µg/mL of RNaseA (Nippon genetics, Tokyo, Japan). The digestion was terminated by adding
440 1% SDS and 22 mM EDTA. The fill-in reaction and biotin labeling steps were omitted from the procedure.
441 The digested genomes were diluted by ligation buffer containing 1% triton-X100 to the final concentration

442 of approximately 1μg/mL and incubated for 10 min at room temperature. Ligation was performed with 2

443 U/mL of T4 DNA ligase (Nippon Gene) overnight at 16˚C. Crosslinking was reversed under 65˚C for 4

444 hours in the presence of 2.5 mg/mL of proteinase K (Kanto Chemical, Tokyo, Japan), and DNA was purified

445 with the phenol-chloroform method and ethanol precipitation method.

446 **Preparation of calibration samples for 3C qPCR**

447 Based on a previous study, calibration samples for possible ligated pairs were prepared in parallel with 3C

448 ligation (58). In brief, the purified genome of *Synechocystis* was digested by HindIII, and DNA was purified

449 with the phenol-chloroform and ethanol precipitation. Purified DNA was dissolved into the ligation buffer

450 at a concentration of about 600ng/μL and ligated with 2 U/mL of T4 DNA ligase at 16˚C overnight.

451 **Quantification of crosslinking frequency for 3C assay**

452 Before the real-time PCR assay, we confirmed that each primer set amplified single bands in a ligation-

453 dependent manner by GoTaq Hot Start Green Master Mix (Promega, Madison, WI) (Figure S10). Real-

454 time PCR was performed with StepOnePlus (Applied Biosystems, Foster City, CA) and Fast SYBR Green

455 Master Mix (Thermo Fisher Scientific) according to the manufacturer's instructions. Interaction frequency

456 was calculated by ΔΔCt method using dilution series of calibration samples described above. We confirmed

457 each primer set amplified DNA fragment with a unique Tm value. The amount of the bait fragment

458 containing *hox* operon were quantified and used as an internal control. Supplemental Table S4 contains the

459 list of primers used in the 3C quantification. Interaction frequency for each primer position was calculated

460 as the relative abundance of ligated fragments against the calibration samples and normalized among
461 samples by internal control.

462 **Statistical analysis**

463 Statistical analyses were performed with R version 4.2.2 (59). The "fisher.test" function was used for
464 Fisher's exact test, and p-values < 0.05 were denoted as asterisks in the figure. Multiple comparisons of
465 Fisher's exact test were conducted using "fisher. Multcomp" function in the RVAideMemoire package (60),
466 where p-values were adjusted by the "fdr" method and FDRs <0.05 are shown in the figures. Multiple
467 comparisons of the Wilcoxon-rank test were conducted by "pairwise.wilcox.test," and p-values were
468 adjusted by the "fdr" method. Adjusted p-values < 0.05 are shown in the figure. The correlation coefficient
469 was calculated with the "cor" function. Gene set enrichment analysis (GSEA) was performed by
470 culsterPlofiler package (61) in R with p-value cut-off of 0.05. The enriched pathways detected by GSEA
471 are listed in Supplemental Table S16.

472 **Manuscript writing**

473 We employed GPT-3.5 to refine the expression of the manuscripts.

474 **Accession Numbers**

475 Raw ChIP sequencing and RNA sequencing reads were deposited in the Sequence Read Archive (accession
476 ID: PRJNA956842).

477

Declaration of interest

The authors declare no competing interests.

Acknowledgments

This study was supported by the following grants to T.O.: Grant-in-Aid for Scientific Research (B) (grant no. 20H02905), JST-ALCA of the Japan Science and Technology Agency (grant number JPMJAL1306), the Asahi Glass Foundation, and JST-GteX (grant number JPMJGX23B0). We thank Dr. Kohki Yoshimoto for providing laboratory instruments and Ms. Kaori Iwazumi for the support of bacterial culture and the medium preparation.

Author contributions

R.K. and T.O. designed the study; R.K. conducted the experiment; R.K. analyzed the data; R.K. and T.O. wrote the paper.

References

1. L. J. Stal, R. Moezelaar, Fermentation in cyanobacteria. *FEMS Microbiol. Rev.* **21**, 179–211 (1997).

2. T. Osanai, *et al.*, Genetic manipulation of a metabolic enzyme and a transcriptional regulator increasing succinate excretion from unicellular cyanobacterium . *Front. Microbiol.* **6**, 1064 (2015).

3. H. Iijima, *et al.*, Metabolomics-based analysis revealing the alteration of primary carbon

496 metabolism by the genetic manipulation of a hydrogenase HoxH in *Synechocystis* sp. PCC 6803.
497 *Algal Res.* **18**, 305–313 (2016).
498 4. M. Akiyama, T. Osanai, Regulation of organic acid and hydrogen production by NADH/NAD(+)
499 ratio in *Synechocystis* sp. PCC 6803. *Front. Microbiol.* **14**, 1332449 (2023).
500 5. D. Carrieri, K. Wawrousek, C. Eckert, J. Yu, P.-C. Maness, The role of the bidirectional
501 hydrogenase in cyanobacteria. *Bioresour. Technol.* **102**, 8368–8377 (2011).
502 6. V. Puggioni, S. Tempel, A. Latifi, Distribution of Hydrogenases in Cyanobacteria: A Phylum-Wide
503 Genomic Survey. *Front. Genet.* **7**, 223 (2016).
504 7. C. Cassier-Chauvat, T. Veaudor, F. Chauvat, Advances in the function and regulation of
505 hydrogenase in the cyanobacterium *Synechocystis* PCC6803. *Int. J. Mol. Sci.* **15**, 19938–19951
506 (2014).
507 8. K. Gutekunst, *et al.*, The bidirectional NiFe-hydrogenase in *Synechocystis* sp. PCC 6803 is reduced
508 by flavodoxin and ferredoxin and is essential under mixotrophic, nitrate-limiting conditions. *J.*
509 *Biol. Chem.* **289**, 1930–1937 (2014).
510 9. J. H. Artz, *et al.*, The structure and reactivity of the HoxEFU complex from the cyanobacterium
511 *Synechocystis* sp. PCC 6803. *J. Biol. Chem.* **295**, 9445–9454 (2020).
512 10. Y. Wang, *et al.*, Pyruvate:ferredoxin oxidoreductase and low abundant ferredoxins support aerobic
513 photomixotrophic growth in cyanobacteria. *Elife* **11**, 2021.08.27.457892 (2022).

514 11. H. Burgstaller, *et al.*, *Synechocystis* sp. PCC 6803 Requires the Bidirectional Hydrogenase to
515 Metabolize Glucose and Arginine Under Oxic Conditions. *Front. Microbiol.* **13**, 896190 (2022).
516 12. J. Appel, S. Phunpruch, K. Steinmüller, R. Schulz, The bidirectional hydrogenase of *Synechocystis*
517 sp. PCC 6803 works as an electron valve during photosynthesis. *Arch. Microbiol.* **173**, 333–338
518 (2000).
519 13. H. Iijima, *et al.*, Four-carbon dicarboxylic acid production through the reductive branch of the open
520 cyanobacterial tricarboxylic acid cycle in *Synechocystis* sp. PCC 6803. *Metab. Eng.* **65**, 88–98
521 (2021).
522 14. J. Hołówka, J. Zakrzewska-Czerwińska, Nucleoid Associated Proteins: The Small Organizers That
523 Help to Cope With Stress. *Front. Microbiol.* **11**, 590 (2020).
524 15. A. Behle, *et al.*, Manipulation of topoisomerase expression inhibits cell division but not growth
525 and reveals a distinctive promoter structure in Synechocystis. *Nucleic Acids Res.* **50**, 12790–12808
526 (2022).
527 16. T. C. Summerfield, S. Nagarajan, L. A. Sherman, Gene expression under low-oxygen conditions
528 in the cyanobacterium *Synechocystis* sp. PCC 6803 demonstrates Hik31-dependent and -
529 independent responses. *Microbiology* **157**, 301–312 (2011).
530 17. T. Osanai, *et al.*, Positive regulation of sugar catabolic pathways in the cyanobacterium
531 *Synechocystis* sp. PCC 6803 by the group 2 sigma factor sigE. *J. Biol. Chem.* **280**, 30653–30659

532 (2005).

533 18. T. Osanai, *et al.*, Genetic engineering of group 2 sigma factor SigE widely activates expressions of

534 sugar catabolic genes in *Synechocystis* species PCC 6803. *J. Biol. Chem.* **286**, 30962–30971 (2011).

535 19. J. Dutheil, *et al.*, The AbrB2 autorepressor, expressed from an atypical promoter, represses the

536 hydrogenase operon to regulate hydrogen production in *Synechocystis* strain PCC6803. *J. Bacteriol.*

537 **194**, 5423–5433 (2012).

538 20. C. Leplat, *et al.*, Genome-wide transcriptome analysis of hydrogen production in the

539 cyanobacterium Synechocystis: Towards the identification of new players. *Int. J. Hydrogen Energy*

540 **38**, 1866–1872 (2013).

541 21. P. Oliveira, P. Lindblad, An AbrB-Like protein regulates the expression of the bidirectional

542 hydrogenase in *Synechocystis* sp. strain PCC 6803. *J. Bacteriol.* **190**, 1011–1019 (2008).

543 22. K. Gutekunst, *et al.*, LexA regulates the bidirectional hydrogenase in the cyanobacterium

544 *Synechocystis* sp. PCC 6803 as a transcription activator. *Mol. Microbiol.* **58**, 810–823 (2005).

545 23. P. Oliveira, P. Lindblad, LexA, a transcription regulator binding in the promoter region of the

546 bidirectional hydrogenase in the cyanobacterium *Synechocystis* sp. PCC 6803. *FEMS Microbiol.*

547 *Lett.* **251**, 59–66 (2005).

548 24. S. Imamura, M. Asayama, Sigma factors for cyanobacterial transcription. *Gene Regul. Syst. Bio.* **3**,

549 65–87 (2009).

550 25. R. Kariyazono, T. Osanai, Identification of the genome-wide distribution of cyanobacterial group-
551 2 sigma factor SigE, accountable for its regulon. *Plant J.* **110**, 548–561 (2022).
552 26. A. Higo, E. Nishiyama, K. Nakamura, Y. Hihara, S. Ehira, cyAbrB Transcriptional Regulators as
553 Safety Devices To Inhibit Heterocyst Differentiation in Anabaena sp. Strain PCC 7120. *J.*
554 *Bacteriol.* **201** (2019).
555 27. A. Ishii, Y. Hihara, An AbrB-like transcriptional regulator, Sll0822, is essential for the activation
556 of nitrogen-regulated genes in *Synechocystis* sp. PCC 6803. *Plant Physiol.* **148**, 660–670 (2008).
557 28. J. Lieman-Hurwitz, *et al.*, A cyanobacterial AbrB-like protein affects the apparent photosynthetic
558 affinity for CO2 by modulating low-CO2-induced gene expression. *Environ. Microbiol.* **11**, 927–
559 936 (2009).
560 29. Y. Yamauchi, Y. Kaniya, Y. Kaneko, Y. Hihara, Physiological roles of the cyAbrB transcriptional
561 regulator pair Sll0822 and Sll0359 in *Synechocystis* sp. strain PCC 6803. *J. Bacteriol.* **193**, 3702–
562 3709 (2011).
563 30. A. Hishida, *et al.*, CRISPRi knockdown of the cyabrB1 gene induces the divergently transcribed
564 icfG and sll1783 operons related to carbon metabolism in the cyanobacterium *Synechocystis* sp.
565 PCC 6803. *J. Gen. Appl. Microbiol.* (2024) https:/doi.org/10.2323/jgam.2024.01.001.
566 31. M. Kopf, *et al.*, Comparative genome analysis of the closely related *Synechocystis* strains PCC
567 6714 and PCC 6803. *DNA Res.* **21**, 255–266 (2014).

568 32. K. Uyeda, J. C. Rabinowitz, Pyruvate-ferredoxin oxidoreductase. 3. Purification and properties of
569 the enzyme. *J. Biol. Chem.* **246**, 3111–3119 (1971).
570 33. P. M. Vignais, B. Billoud, Occurrence, classification, and biological function of hydrogenases: an
571 overview. *Chem. Rev.* **107**, 4206–4272 (2007).
572 34. M. Ortega-Ramos, *et al.*, Engineering *Synechocystis* PCC6803 for hydrogen production: influence
573 on the tolerance to oxidative and sugar stresses. *PLoS One* **9**, e89372 (2014).
574 35. N. Katayama, K. Iwazumi, H. Suzuki, T. Osanai, S. Ito, Malic Enzyme, not Malate Dehydrogenase,
575 Mainly Oxidizes Malate That Originates from the Tricarboxylic Acid Cycle in Cyanobacteria.
576 *MBio* **13**, e0218722 (2022).
577 36. S. A. Angermayr, *et al.*, Chirality Matters: Synthesis and Consumption of the d-Enantiomer of
578 Lactic Acid by *Synechocystis* sp. Strain PCC6803. *Appl. Environ. Microbiol.* **82**, 1295–1304
579 (2016).
580 37. W. W. Navarre, M. McClelland, S. J. Libby, F. C. Fang, Silencing of xenogeneic DNA by H-NS-
581 facilitation of lateral gene transfer in bacteria by a defense system that recognizes foreign DNA.
582 *Genes Dev.* **21**, 1456–1471 (2007).
583 38. T. Oshima, S. Ishikawa, K. Kurokawa, H. Aiba, N. Ogasawara, Escherichia coli Histone-Like
584 Protein H-NS Preferentially Binds to Horizontally Acquired DNA in Association with RNA
585 Polymerase. *DNA Res.* **13**, 141–153 (2006).

586 39. B. R. G. Gordon, *et al.*, Lsr2 is a nucleoid-associated protein that targets AT-rich sequences and
587 virulence genes in Mycobacterium tuberculosis. *Proc. Natl. Acad. Sci.* **107**, 5154–5159 (2010).
588 40. M. Kołodziej, *et al.*, Lsr2 and Its Novel Paralogue Mediate the Adjustment of Mycobacterium
589 smegmatis to Unfavorable Environmental Conditions. *mSphere* **6** (2021).
590 41. K. Song, *et al.*, Expression of the Cyanobacterial F(o)F(1) ATP Synthase Regulator AtpΘ Depends
591 on Small DNA-Binding Proteins and Differential mRNA Stability. *Microbiol. Spectr.* **10**,
592 e0256221 (2022).
593 42. P. Spät, V. Krauspe, W. R. Hess, B. Maček, N. Nalpas, Deep Proteogenomics of a Photosynthetic
594 Cyanobacterium. *J. Proteome Res.* **22**, 1969–1983 (2023).
595 43. S. Sakr, *et al.*, The activity of the *Synechocystis* PCC6803 AbrB2 regulator of hydrogen production
596 can be post-translationally controlled through glutathionylation. *Int. J. Hydrogen Energy* **38**,
597 13547–13555 (2013).
598 44. D. Camsund, T. Heidorn, P. Lindblad, Design and analysis of LacI-repressed promoters and DNA-
599 looping in a cyanobacterium. *J. Biol. Eng.* **8**, 4 (2014).
600 45. T. Osanai, *et al.*, ChlH, the H subunit of the Mg-chelatase, is an anti-sigma factor for SigE in
601 *Synechocystis* sp. PCC 6803. *Proc. Natl. Acad. Sci. U. S. A.* **106**, 6860–6865 (2009).
602 46. H. Iijima, *et al.*, Changes in primary metabolism under light and dark conditions in response to
603 overproduction of a response regulator RpaA in the unicellular cyanobacterium *Synechocystis* sp.

604 PCC 6803 . *Front. Microbiol.* **6**, 888 (2015).

605 47. J. G. K. Williams, "Construction of Specific Mutations in Photosystem II Photosynthetic Reaction

606 Center by Genetic Engineering Methods in *Synechocystis* 6803" in *Methods in Enzymology*,

607 (Academic Press, 1988), pp. 766–778.

608 48. R. Rippka, J. Deruelles, J. B. Waterbury, Generic assignments, strain histories and properties of

609 pure cultures of cyanobacteria. *J. Gen. Microbiol.* **111**, 1–61 (1979).

610 49. S. Chen, Y. Zhou, Y. Chen, J. Gu, fastp: an ultra-fast all-in-one FASTQ preprocessor.

611 *Bioinformatics* **34**, i884–i890 (2018).

612 50. B. Langmead, S. L. Salzberg, Fast gapped-read alignment with Bowtie 2. *Nat. Methods* **9**, 357–359

613 (2012).

614 51. S. Anders, P. T. Pyl, W. Huber, HTSeq--a Python framework to work with high-throughput

615 sequencing data. *Bioinformatics* **31**, 166–169 (2015).

616 52. M. D. Robinson, D. J. McCarthy, G. K. Smyth, edgeR: a Bioconductor package for differential

617 expression analysis of digital gene expression data. *Bioinformatics* **26**, 139–140 (2010).

618 53. Y. Zhang, *et al.*, Model-based analysis of ChIP-Seq (MACS). *Genome Biol.* **9**, R137 (2008).

619 54. A. R. Quinlan, I. M. Hall, BEDTools: a flexible suite of utilities for comparing genomic features.

620 *Bioinformatics* **26**, 841–842 (2010).

621 55. W. Shen, S. Le, Y. Li, F. Hu, SeqKit: A Cross-Platform and Ultrafast Toolkit for FASTA/Q File

622 Manipulation. *PLoS One* **11**, e0163962 (2016).

623 56. N. Takemata, R. Y. Samson, S. D. Bell, Physical and Functional Compartmentalization of Archaeal

624 Chromosomes. *Cell* **179**, 165-179.e18 (2019).

625 57. N. Takemata, S. D. Bell, Chromosome conformation capture assay combined with biotin

626 enrichment for hyperthermophilic archaea. *STAR Protoc.* **2**, 100576 (2021).

627 58. M. Abou El Hassan, R. Bremner, A rapid simple approach to quantify chromosome conformation

628 capture. *Nucleic Acids Res.* **37**, e35 (2009).

629 59. , R: A Language and Environment for Statistical Computing (2022).

630 60. M. Hervé, RVAideMemoire: Testing and Plotting Procedures for Biostatistics (2022).

631 61. T. Wu, *et al.*, clusterProfiler 4.0: A universal enrichment tool for interpreting omics data. *Innov.*

632 *(Cambridge* **2**, 100141 (2021).

633

634 **Table 1** List of transiently upregulated genes

		Operon
Oxidoreductase		
sll0741	*nifJ*/"pyruvate-ferredoxin/flavodoxin oxidoreductase"	TU3296
sll0743	hypothetical protein	
sll0744	dihydroorotate dehydrogenase (fumarate)	
sll1221	*hoxF*/“bidirectional [NiFe] hydrogenase diaphorase subunit”	TU1714
sll1222	unknown protein	
sll1223	*hoxU*/“bidirectional [NiFe] hydrogenase diaphorase subunit”	
sll1224	*hoxY*/“NAD-reducing hydrogenase small subunit”	
sll1225	unknown protein	
sll1226	*hoxH*/“NAD-reducing hydrogenase large subunit”	
slr1434	*pntB*/"H+-translocating NAD(P) transhydrogenase subunit beta"	TU1089
Transporter		
sll1450	*nrtA*/“nitrate/nitrite transport system substrate-binding protein”	TU1023
sll1451	*nrtB*/“nitrate/nitrite transport system permease protein”	
sll1452	*nrtC*/“nitrate/nitrite transport system ATP-binding protein”	
sll1453	*nrtD*/“nitrate/nitrite transport system ATP-binding protein”	
Two-component system		
slr1214	twitching motility two-component system response regulator PilG	TU905
slr1215	unknown protein	TU907
Glycosyl transferase		
slr2116	*spsA*/“spore coat polysaccharide biosynthesis protein; SpsA”	TU1673

Protease		
sll1009	*frpC*/"iron-regulated protein"	TU491
Insertion sequence (Transposase)		
slr1523	transposase	TU1659
sll1985	transposase	TU1589
sll7001	transposase	NA
sll7003	toxin FitB	TU7001
ssl0172	transposase	TU3163
Other		
slr1260	hypothetical protein	TU1446
slr0668	unknown protein	TU3532
slr5127	unknown protein	TU5127
sll0710	unknown protein	TU97
sll1307	unknown protein	TU1224

635 The list of transiently upregulated genes was merged by transcriptional units and sorted by function. The

636 transcriptional unit information was obtained from a previous study (Kopf et al., 2014).

637

638

639 **Figures and Figure legends**

Figure 1

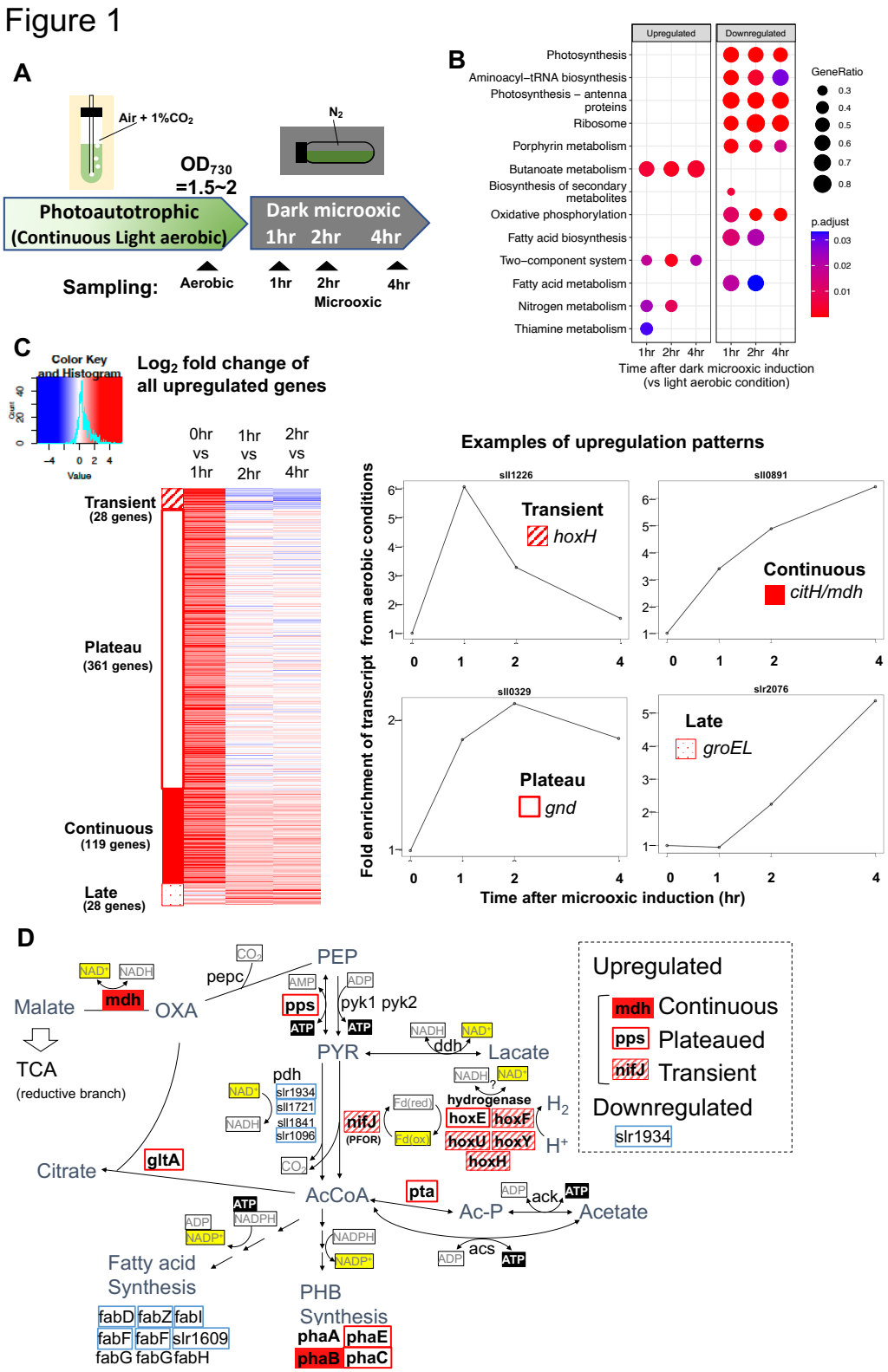

640

641 **Figure 1**

642 (A) Schematic diagram for the sampling of cells under aerobic and microoxic conditions. (B) Gene set

643 enrichment analysis on time-course transcriptome data. KEGG pathways enriched in upregulated or

644 downregulated genes after 1-, 2-, and 4-h incubation under microoxic conditions are shown. (C) (left)

645 Heatmap showing expression change in all upregulated genes over the time-course. Genes classified into

646 Transient (striped square), Plateau (open square), Continuous (filled square), and Late (dotty square) were

647 clustered into subgroups and sorted by the gene name. (right) Examples of genes are classified into each

648 expression pattern. (D) The classified genes were mapped to central carbon metabolism, centered on

649 pyruvate. PEP: phosphoenolpyruvate, PYR: pyruvate, AcCoA: acetyl CoA, Ac-P: acetyl phosphate,

650 OXA: oxaloacetate, PHB: polyhydroxy butyrate. TCA: tricarboxylic acid cycle.

651

Figure 2

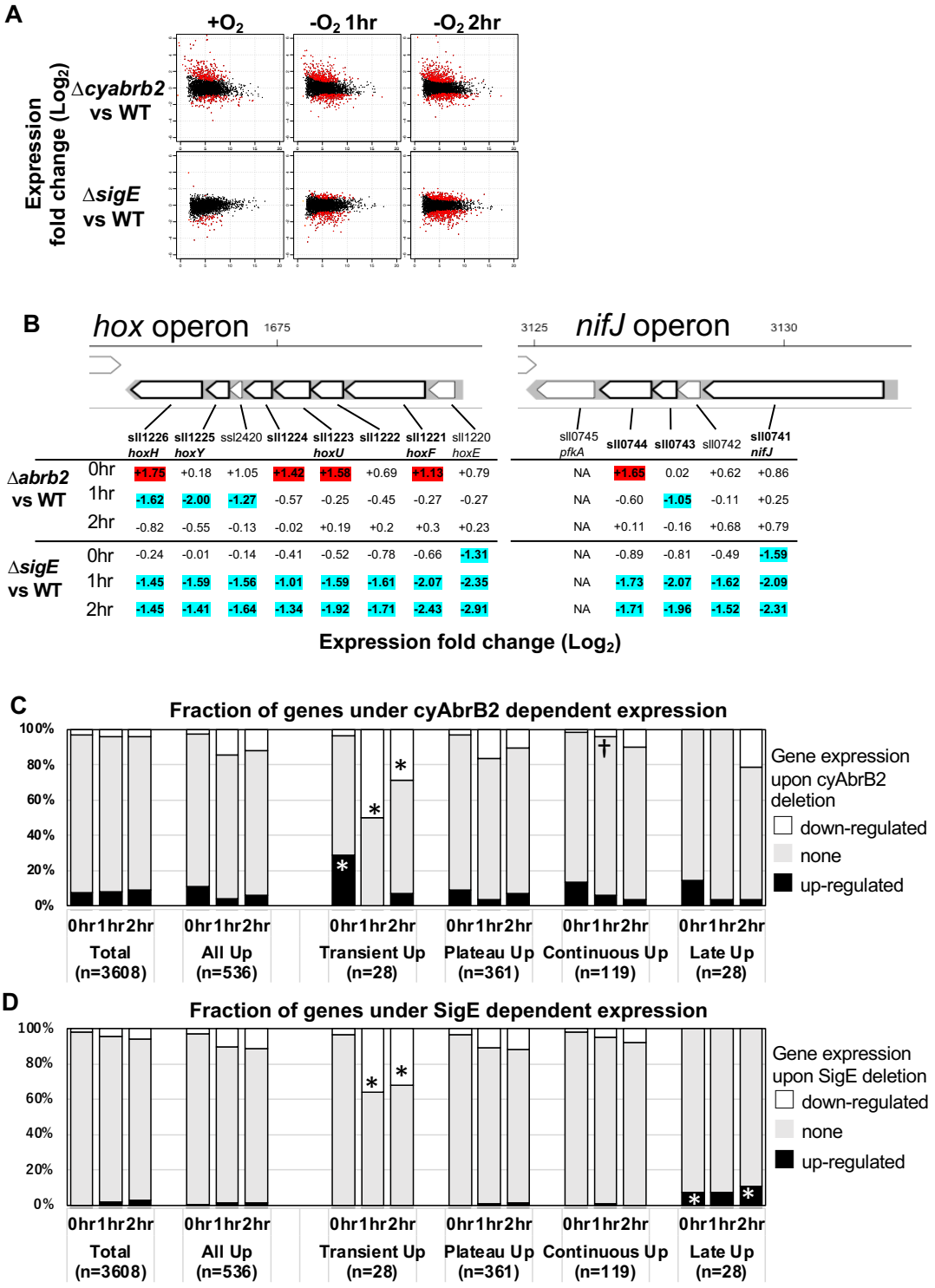

Figure 2

(A) MA plot showing fold change (y-axis) and average (x-axis) of gene expression between wildtype and

655 mutant strains at each timepoint. Red dots indicate defined DEGs (|Log_2 FC| >1 with FDR < 0.05). (B)

656 Log2 scaled expression fold change in genes in the *hox* and *nifJ* operons upon Δ*cyabrb2* and Δ*sigE* under

657 aerobic conditions (0 h), 1 hour after microoxic condition (1 hr), and 2 hours after microoxic condition (2

658 hr). DEGs are marked with sky blue (downregulated upon deletion) or red (upregulated upon deletion).

659 (C and D) Fraction of upregulated and downregulated genes upon the (C) Δ*cyabrb2* and (D) Δ*sigE* at the

660 timepoints of aerobic conditions (0 hr), 1 hour after anoxic condition (1 hr), and 2 hour after anoxic

661 condition (2 hr). Genes are classified according to Figure 1C. Asterisk (*) and dagger (†) denote

662 statistically significant enrichment and anti-enrichment compared with all upregulated genes tested by

663 multiple comparisons of Fisher's exact test (FDR < 0.05).

664

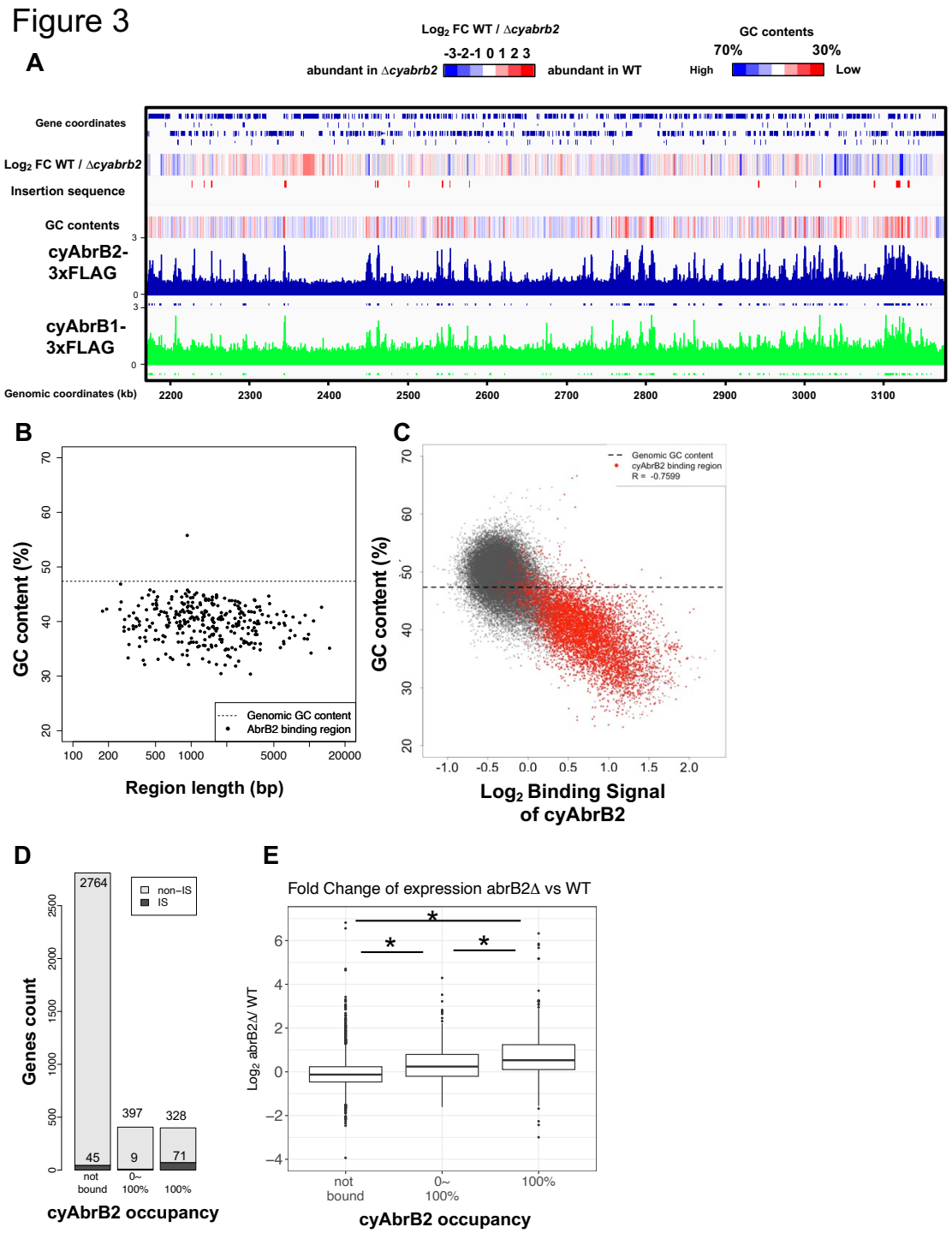

Figure 3

(A) Snapshot of ChIP-seq data for cyAbrB2 and cyAbrB1 under aerobic conditions. The heatmap in the second column indicates expression fold change upon Δ*cyabrb2* under aerobic conditions. Positive values

669 (colored in red) indicate that the gene expression is higher in wildtype than in Δ*cyabrb2*, and negative

670 values (colored in blue) indicate the opposite. The positions for the insertion elements are marked with

671 red in the third column. The heatmap in the fourth column indicates GC contents. High GC contents are

672 colored in blue and low GC contents are colored in blue. (B) GC contents and region length of cyAbrB2

673 binding regions (black dots). The horizontal dotted line indicates the genomic average of GC content. (C)

674 Scatter plot of GC content and binding signal of cyAbrB2. The x-axis is the binding signal of cyAbrB2 in

675 each 100 bp region, and the y-axis indicates GC contents within 500 bp windows sliding every 100 base

676 pairs. CyAbrB2 binding regions are marked with red dots. (D) Histogram of genes showing the extent of

677 occupancy (not bound, partially overlapped, or entirely overlapped) by the cyAbrB2 binding region. The

678 gray bars indicate non-IS genes, and the count numbers of the non-IS genes are displayed on the gray

679 bars. The black bars indicate the IS genes, and the count numbers of the IS genes are displayed above the

680 black bars. (E) Boxplot showing fold change in gene expression by Δ*cyabrb2* under aerobic conditions.

681 Genes are classified according to the extent of occupancy by the cyAbrB2 binding region. Asterisk (*)

682 denotes statistical significance tested by multiple comparisons of the Wilcoxon-rank test.

683

Figure 4

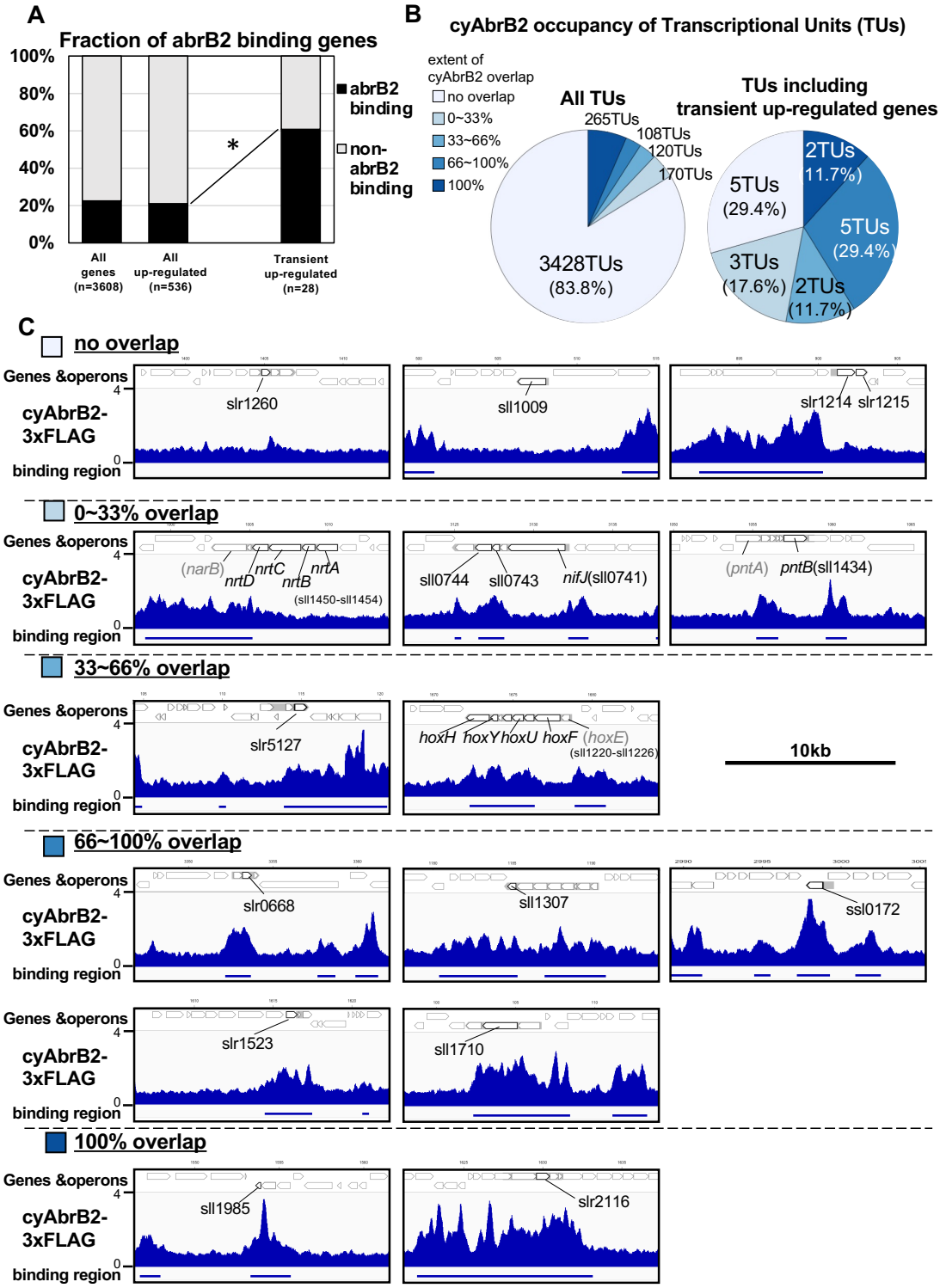

Figure 4

686 (A) Fraction of genes overlapped or non-overlapped with cyAbrB2 binding regions at the timepoints of
687 aerobic conditions. Genes are classified according to Figure S1. Asterisk (*) denotes statistically
688 significant enrichment compared with all upregulated genes tested by multiple comparisons of Fisher's
689 exact test. (B) Pie charts of transcriptional units (TUs) classified by extent of overlapping with cyAbrB2
690 binding region. The left pie represents all TUs, and the right pie represents only TUs containing the
691 transient upregulated genes. (C) Distribution of cyAbrB2 in the aerobic condition around transiently
692 upregulated genes. Arrows with bold lines indicate transiently upregulated genes. Shaded arrows indicate
693 operons whose data were obtained from a previous study. The bars below the graph indicate the binding
694 regions of each protein. The black bar at the top of the figure indicates a length of 10 kbp.
695

696

Figure 5

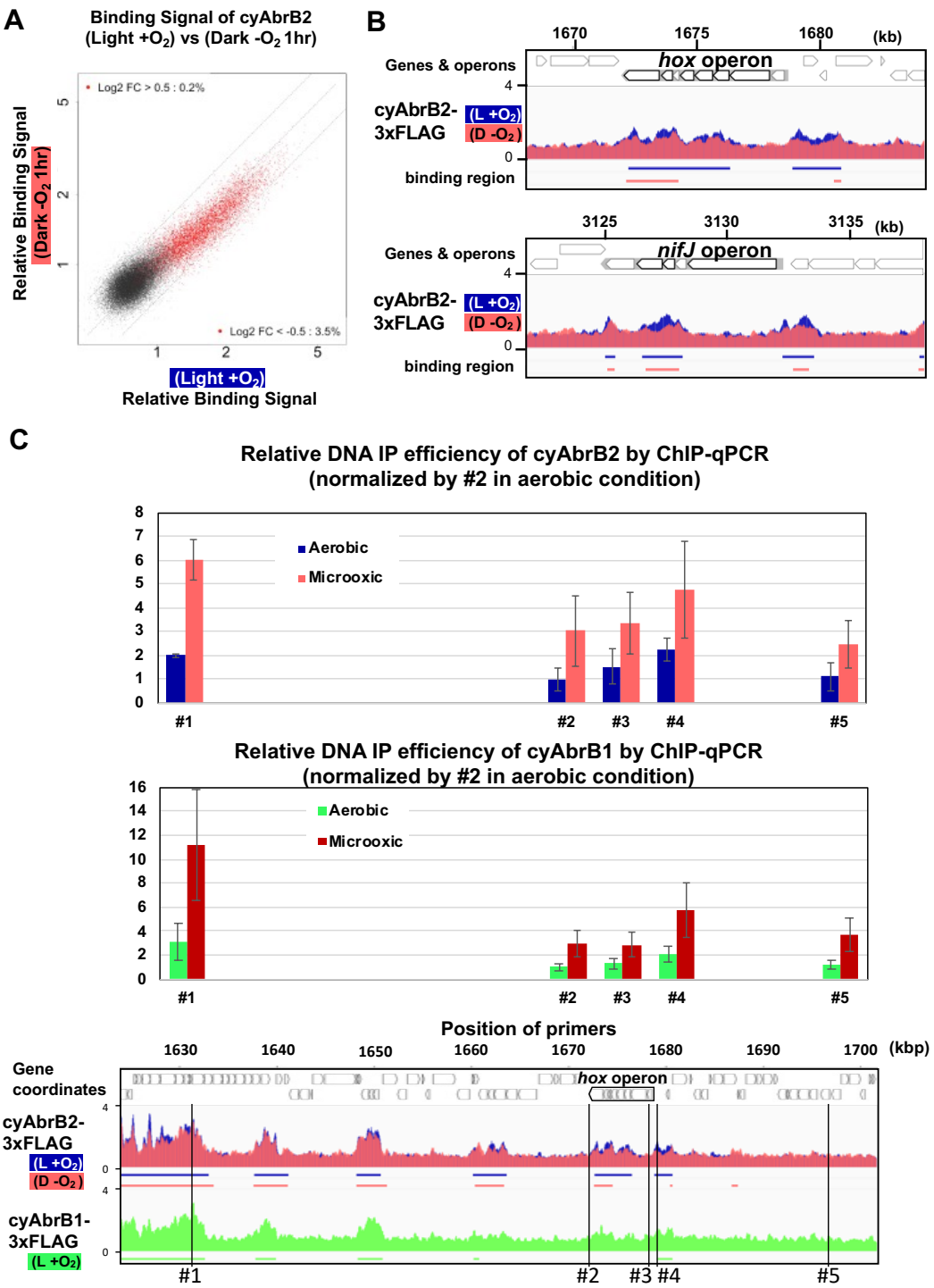

697

698 **Figure 5**

699 (A) Scatter plot showing changes of the binding signal by 1hr cultivation in the microoxic condition. The

700 binding signal of each 100bp window is plotted. Red dots are cyAbrB2 binding regions in either aerobic

701 or microoxic conditions. The dotty lines indicate Log2 fold enrichment of 0.5, 0, and -0.5 between

702 aerobic and microoxic conditions. (B) Distribution of cyAbrB2 around *hox* operon and *nifJ* operon. ChIP-

703 seq data in aerobic (L + O_2) and dark microoxic (D − O_2) conditions are overlayed. The bars below the

704 graph indicate the binding regions of each protein. (C) Quantification for IP efficiency of cyAbrB2 (top)

705 and cyAbrB1 (middle) by qPCR in the aerobic and microoxic conditions. The position of primers and

706 ChIP-seq data of cyAbrB2 are shown at the bottom. Scores are normalized by the IP% at position #2 in

707 the aerobic condition.

708

709

Figure 6

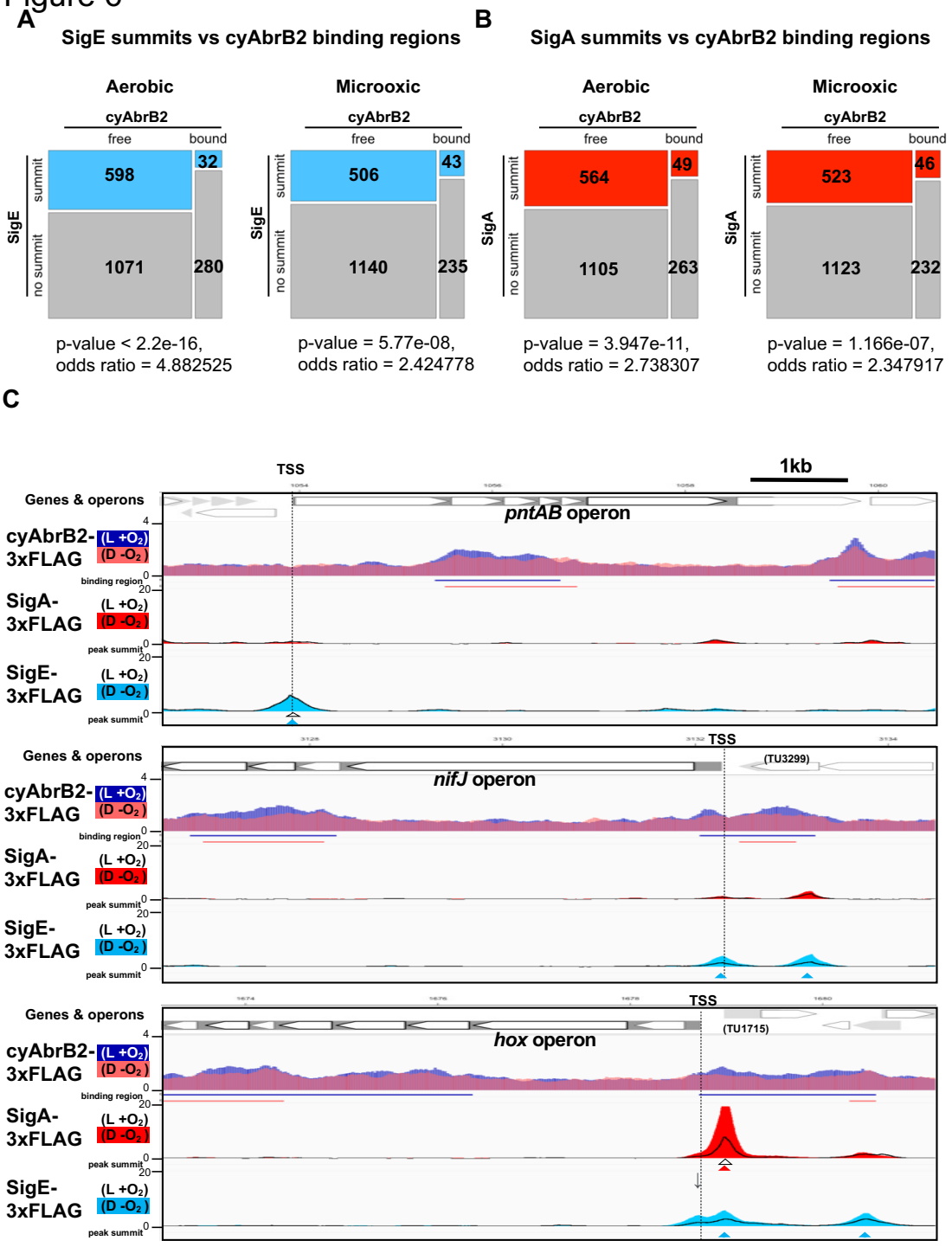

Figure 6

(A, B) Anti-co-occurrence of cyAbrB2 binding regions and sigma factors. Mosaic plots of cyAbrB2 binding regions and SigE peaks (A) or SigA binding peaks (B) are shown. Odds and p-values were

714 calculated by Fisher's exact test. (C) Snapshots of ChIP-seq data for CyAabrB2, SigE, and SigA at the

715 *nifJ* region (top) and *hox* region (bottom). ChIP-seq data for cyAbrB2, SigE, and SigA under aerobic and

716 dark microoxic conditions are overlayed. ChIP-seq data of cyAbrB2 under aerobic and microoxic

717 conditions are colored blue and pink, respectively. ChIP-seq data for SigE and SigA are shown in solid

718 lines (aerobic conditions) and the area charts (microoxic conditions). The positions of TSSs were obtained

719 from a previous study (Kopf et al., 2014) and indicated by vertical dotted lines. Open triangles indicate

720 peak summits under aerobic conditions, and solid triangles indicate peak summits under microoxic

721 conditions.

Figure 7

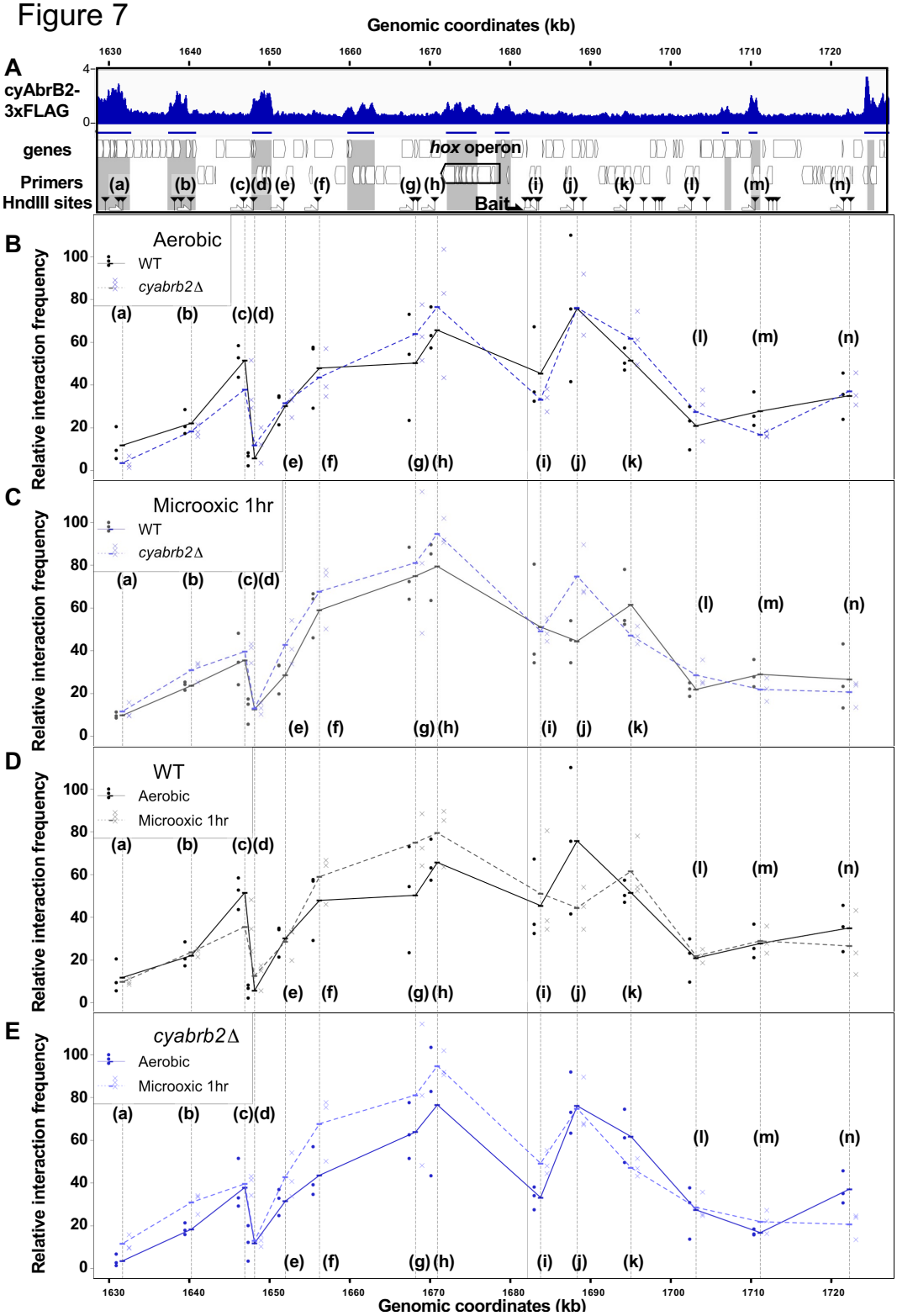

722

723

Figure 7 (continued)

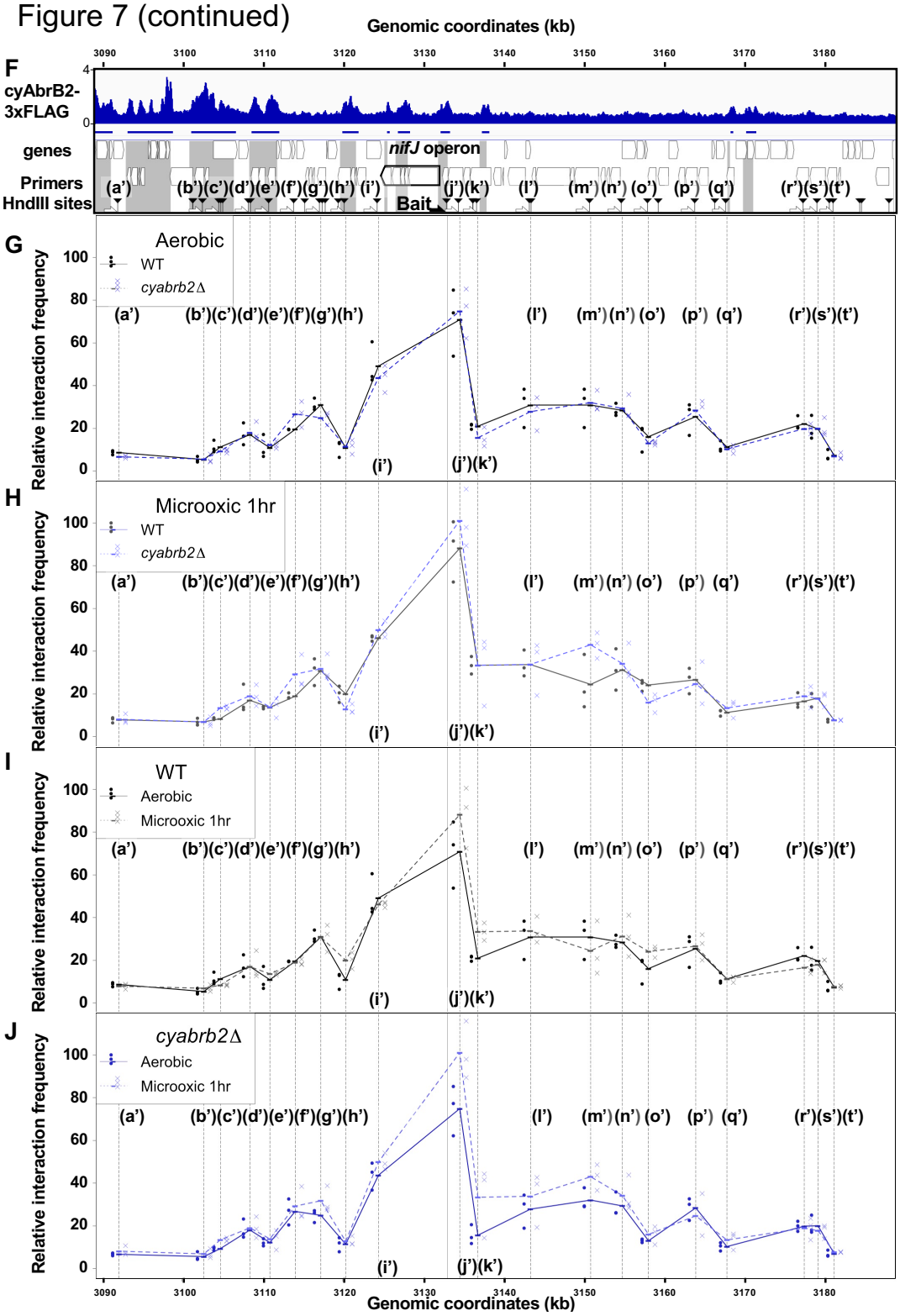

Figure 7

726 (A) and (F)Schematic diagram of 3C analysis around *hox* operon (A) and *nifJ* operon (F). In the panels

727 (A) and (F), the black horizontal arrow shows the location of the bait primer, and white horizontal arrows

728 ((a) to (n) in *hox* operon (A) and (a') to (t') in *nifJ* operon (F)) indicate loci where the interaction

729 frequency with bait were assayed. Vertical black arrowheads indicate the position of HindIII sites. ChIP-

730 seq data of cyAbrB2 in the aerobic condition is displayed in the bottom, and cyAbrB2 binding regions are

731 marked with shade. (B - E) The line plot showing the interaction frequency of each locus with *hox*

732 fragment. Two of data sets are presented; (B) wildtype vs Δ*cyabrb2* in aerobic condition, (C) wildtype vs

733 Δ*cyabrb2* in 1hr of microoxic condition, (E) wildtype in aerobic vs 1hr of microoxic condition, and (E)

734 Δ*cyabrb2* in aerobic vs 1hr of microoxic condition are compaired. (G – J) The line plot showing the

735 interaction frequency of each locus with *nifJ* fragment. Two data sets are selected and presented; (G)

736 wildtype vs Δ*cyabrb2* in aerobic condition, (H) wildtype vs Δ*cyabrb2* in 1hr of microoxic condition, (I)

737 wildtype in aerobic vs 1hr of microoxic condition, and (J) Δ*cyabrb2* in aerobic vs 1hr of microoxic

738 conditions are compared. The line plots indicate the average interaction frequency over the random

739 ligation (n=3). Individual data are plotted as dots.

740

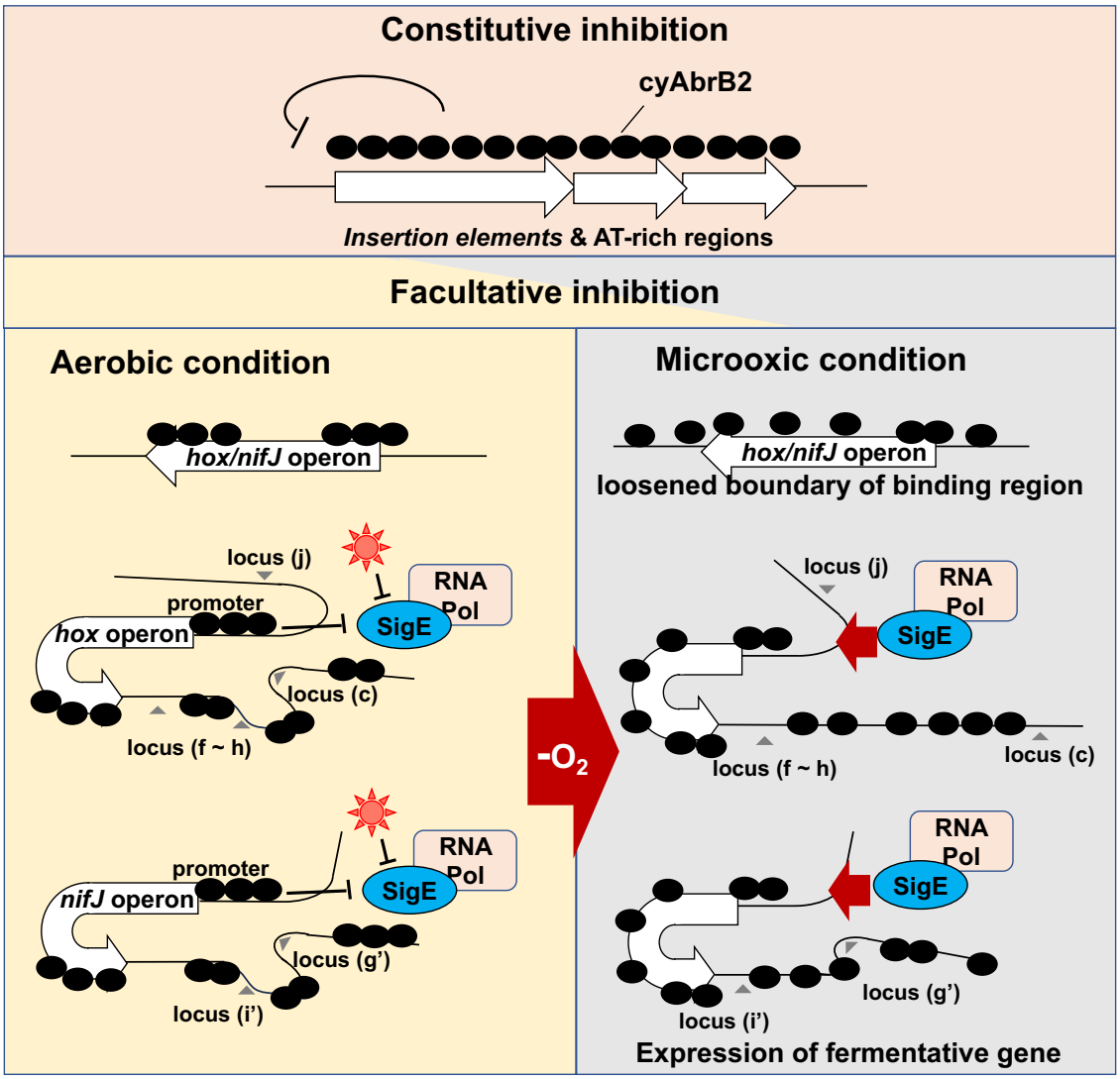

Figure 8

Schematic diagram of the dynamics of transcription factors governing fermentative gene expression.

Figure S1

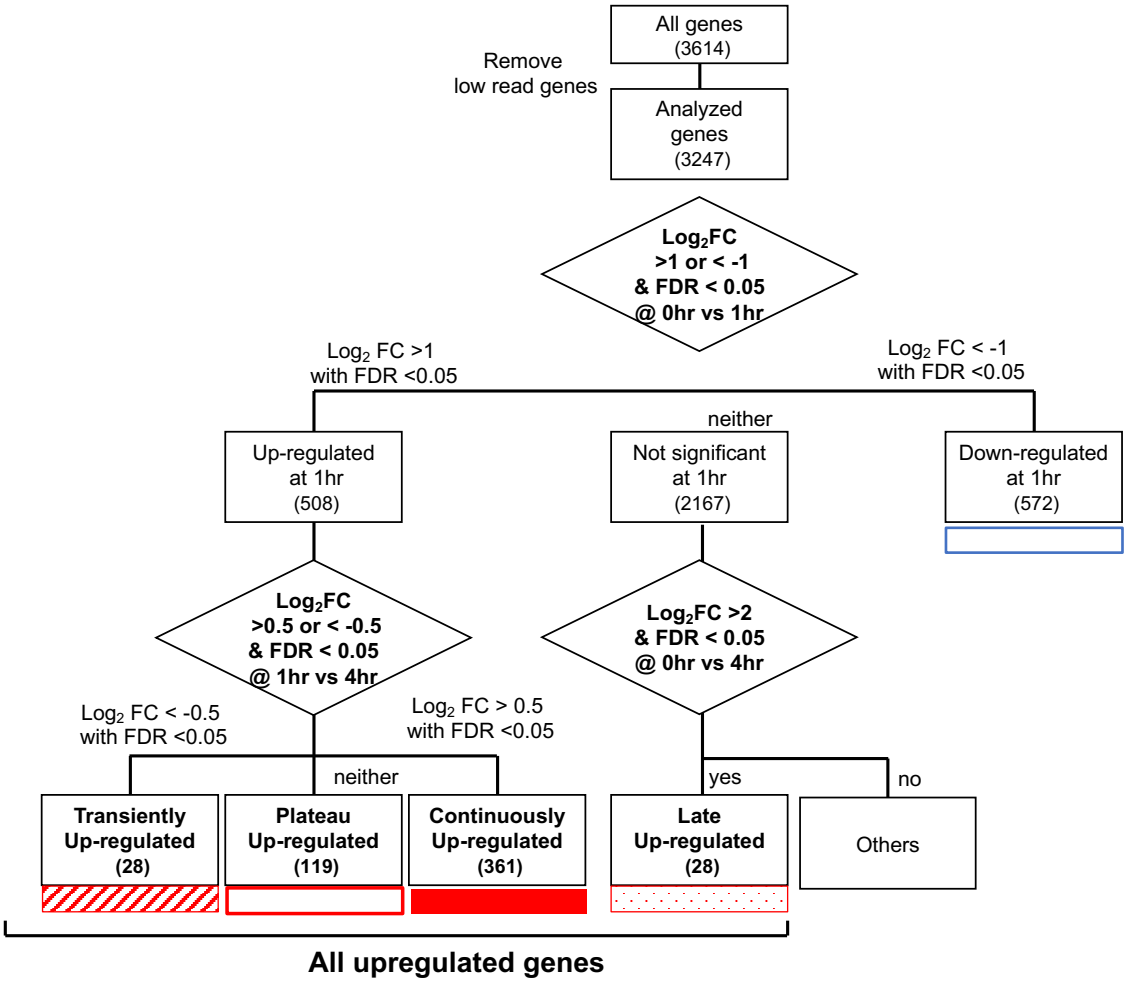

Figure S1

Schematic diagram showing the classification of genes according to the time-course transcriptome. Transient (striped square), Plateau (open square), Continuous (filled square), and Late (dotty square) are denoted as all upregulated genes.

Figure S2

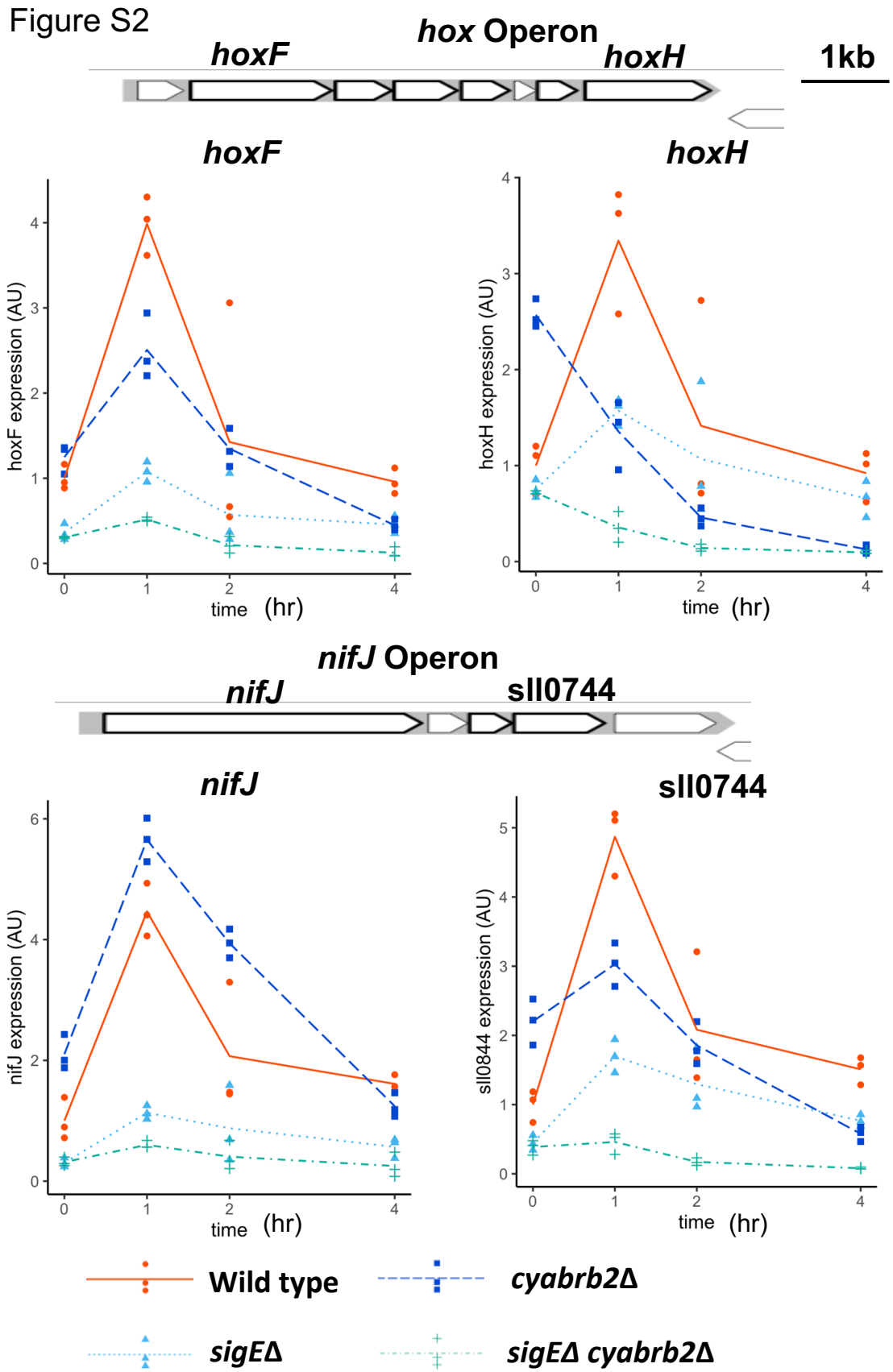

752

753 **Figure S2**

754 RT-qPCR validated the transiently upregulated genes classified by RNAseq. Transcripts extracted from

755 wildtype (solid line), Δ*sigE* mutant (dotty line), Δ*cyabrb2* mutant (dashed line), and Δ*sigE* Δ*cyabrb2*

756 double mutant (dot-dashed line) were assayed in the aerobic condition (0hr) and 1,2,4 hour incubation of

757 microoxic conditions. As the representative of the transiently upregulated genes, expression of *hoxF*,

758 *hoxY, nifJ,* and *sll0744* were quantified by RT-qPCR. The line represents the mean of n=3, and individual

759 data points are shown as dot plots. Data of each gene is normalized by the mean score of wildtypes in the

760 aerobic condition.

761

Figure S3

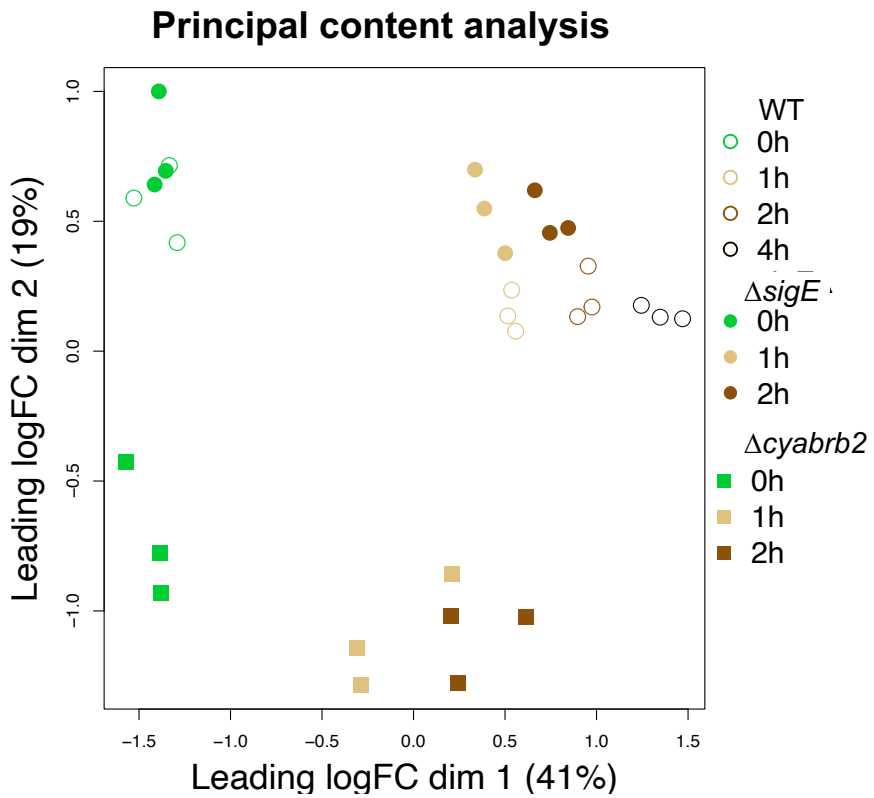

Figure S3

Primary component scatter plot showing the profiles of RNA-seq data.

Figure S4

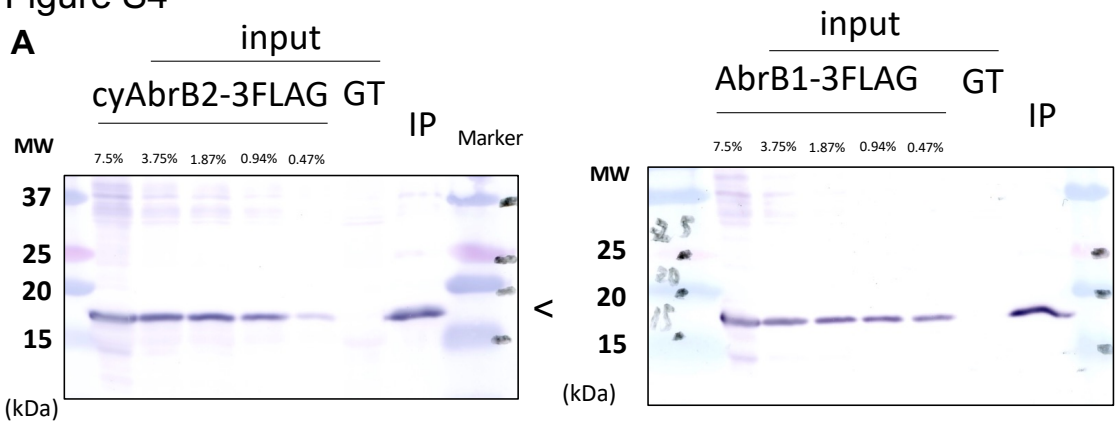

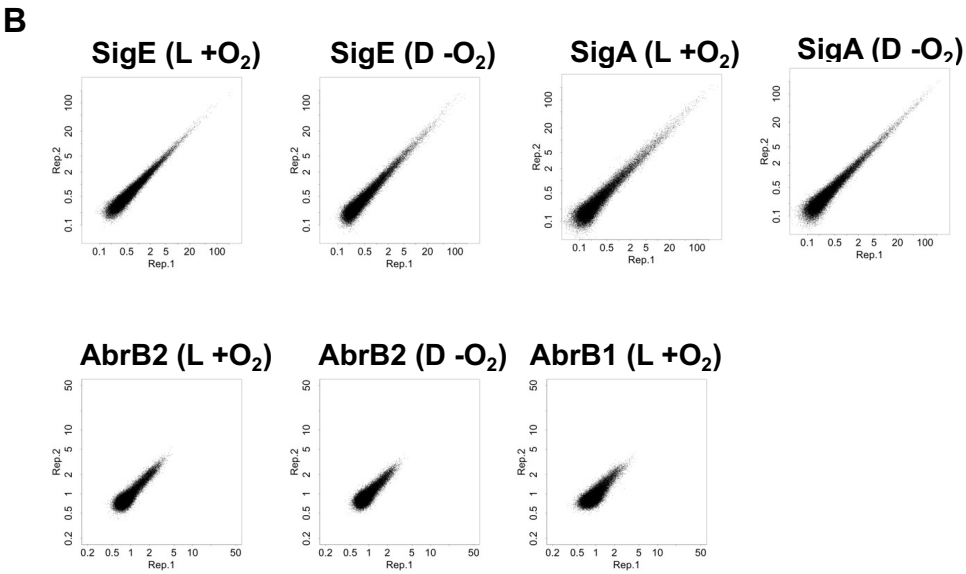

765

Figure S4 (continuing)

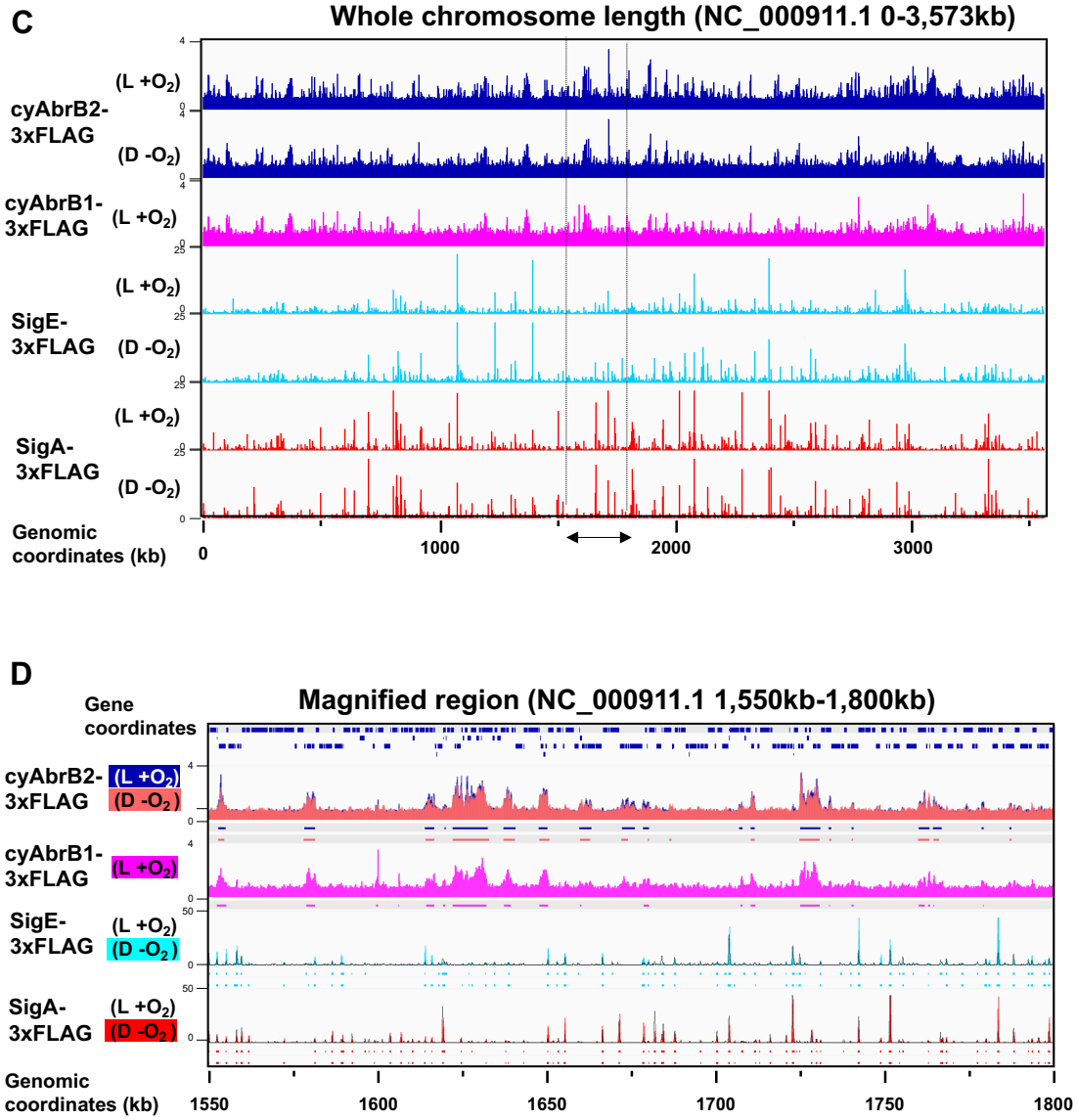

Figure S4 The procedure for ChIP-seq of flag-tagged proteins and Overview of ChIP-seq data

Validation of procedure for ChIP-seq of flag-tagged cyAbrB2, SigE, and SigA.

(A) The immunoblot for inputs and immunoprecipitants (IP) of ChIP for cyAbrB2-FLAG and cyAbrB1-FLAG. Input lysate of untagged control (GT) is also loaded. Inputs equivalent to the indicated portion of IP were loaded. (B)Scatter plots showing the reproducibility of two replicates for ChIP-seq assay. ChIP-

seq data of SigE, SigA, and cyAbrB2 in aerobic and microoxic conditions and ChIP-seq data of cyAbrB1 in the aerobic condition are shown. Dots indicate normalized IP read count / normalized input read count in each 100bp window. X-axis is the value of replicate1, and Y-axis is the value of replicate 2. (C) and (D) Overview for ChIp-seq of flag tagged cyAbrB2, cyAbrB1, SigE, and SigA. Y-axis indicates [normalized IP read count / normalized input read count at each 25bp window], and X-axis indicates chromosome position. (C) Distribution of cyAbrB2, cyAbrB1, SigE, and SigA across the whole genome of *Synechocystis*. Aerobic (L +O_2) and dark microoxic (D -O_2) data are displayed. (D) Magnified image for chromosome position of 1,550kb-1,800kb. ChIP-seq data of cyAbrB2, cyAbrB1, SigE, and SigA in aerobic and dark microoxic conditions are overlayed. The dots below the graph indicate the binding region of each protein calculated by peak caller.

Figure S5

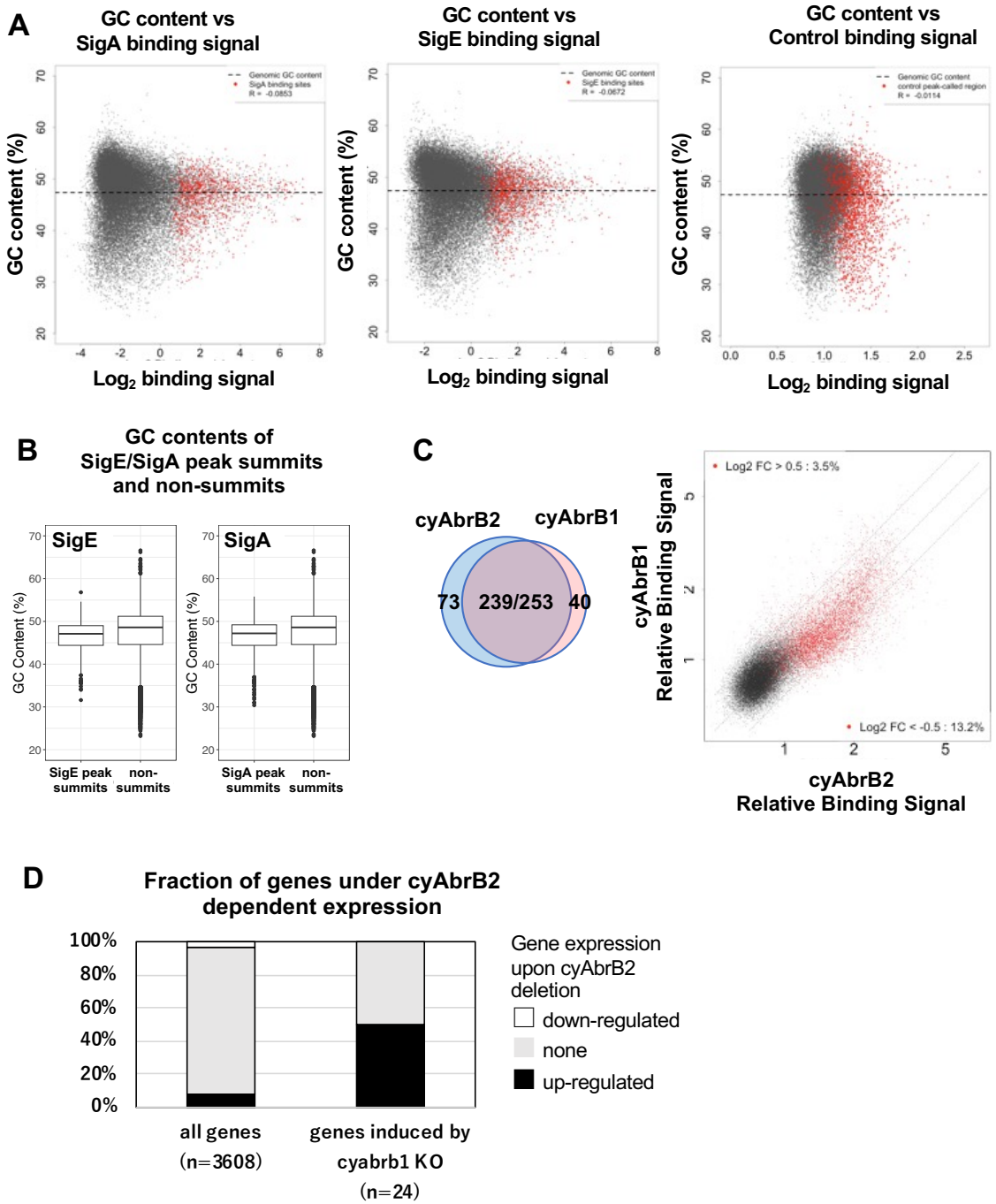

Figure S5 GC content vs ChIP enrichment score of SigA and SigE

(A) Scatter plot showing GC contents in each 100bp vs. binding signal of SigA, SigE, and control IP.

788 Data are displayed as in Figure 3C. (B) GC content in each 100bp of (left) SigE peaks and non-SigE

789 peaks, and (right) SigA peaks and non-SigA peaks. (C) Venn diagram showing overlap of the binding

790 region of cyAbrB1 and cyAbrB2 (left), and scatter plot showing ChIP binding signal of cyAbrB2 (y-axis)

791 and cyAbrB1(x-axis) in the aerobic condition. Data is plotted as in Figure 5A. (D) Fractions of

792 upregulated and downregulated genes upon the Δ*cyabrb2* mutant in the aerobic conditions. Fractions of

793 all genes (left n=3608) and genes induced by cyAbrB1 knockout (right n=24) are shown. Genes induced

794 by cyAbrB1 knockout are from the previous study (30).

795

796

Figure S6

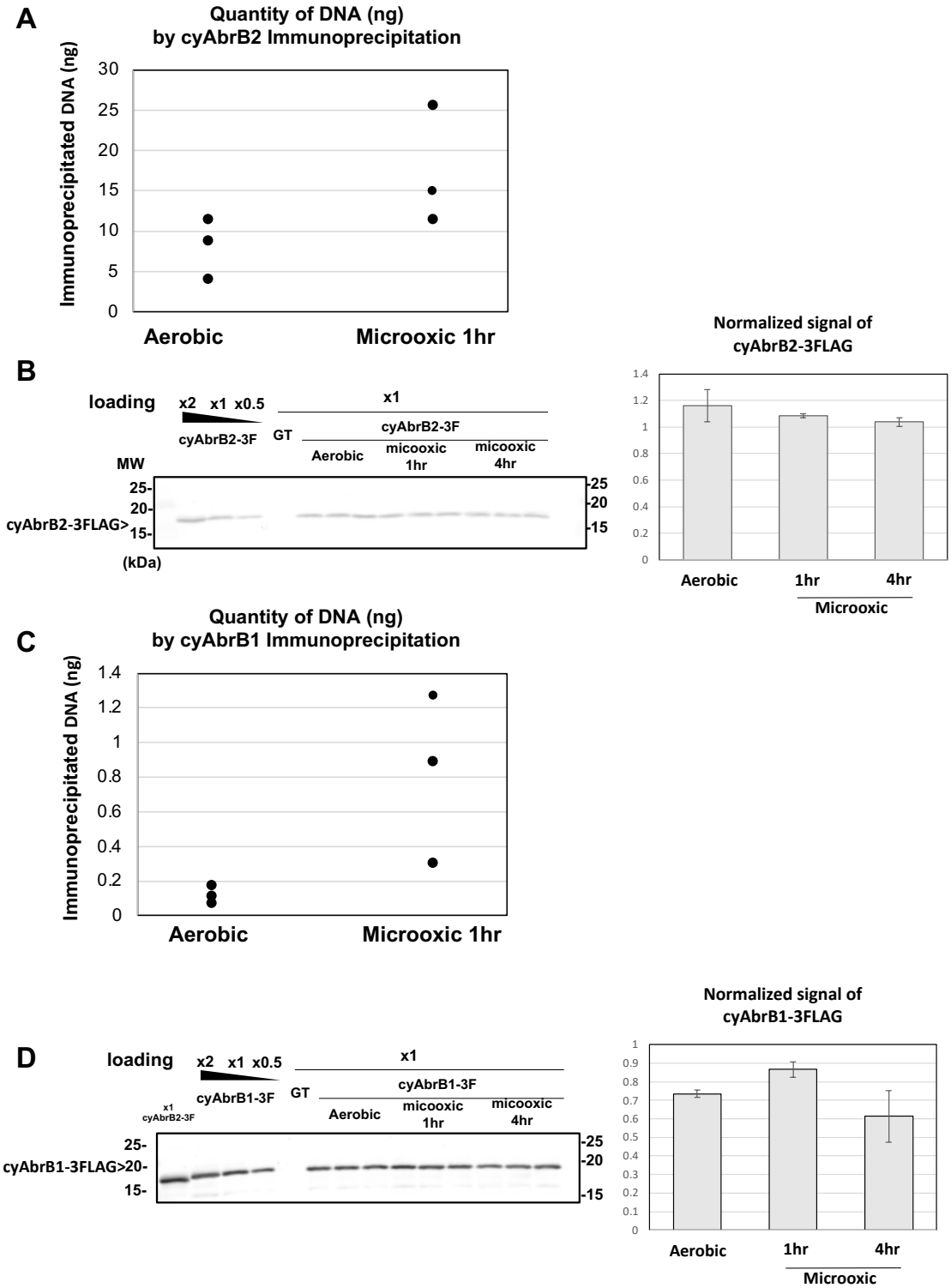

797

798

799 **Figure S6 Alteration of cyAbrB2 binding to genome under the microoxic condition**

800 (A) and (C) Amount of precipitated DNA by cyAbrB2 ChIP and cyAbrB1 ChIP, respectively. Three

801 experiments were performed in the aerobic and microoxic conditions. (B) and (D) Western blot images of

802 cyAbrB2-3FLAG and cyAbrB1-3FLAG, respectively. Proteins were extracted in the aerobic condition

803 and 1hr and 4hr incubation under microoxic conditions. The total protein concentration of each sample

804 was adjusted to 4mg/mL, measured by the BCA method. Quantification of cyAbrB2 from western blot

805 image was performed by ImageJ (ver. 2.0.0-rc-65) and plotted in the right graph.

806

807

Figure S7

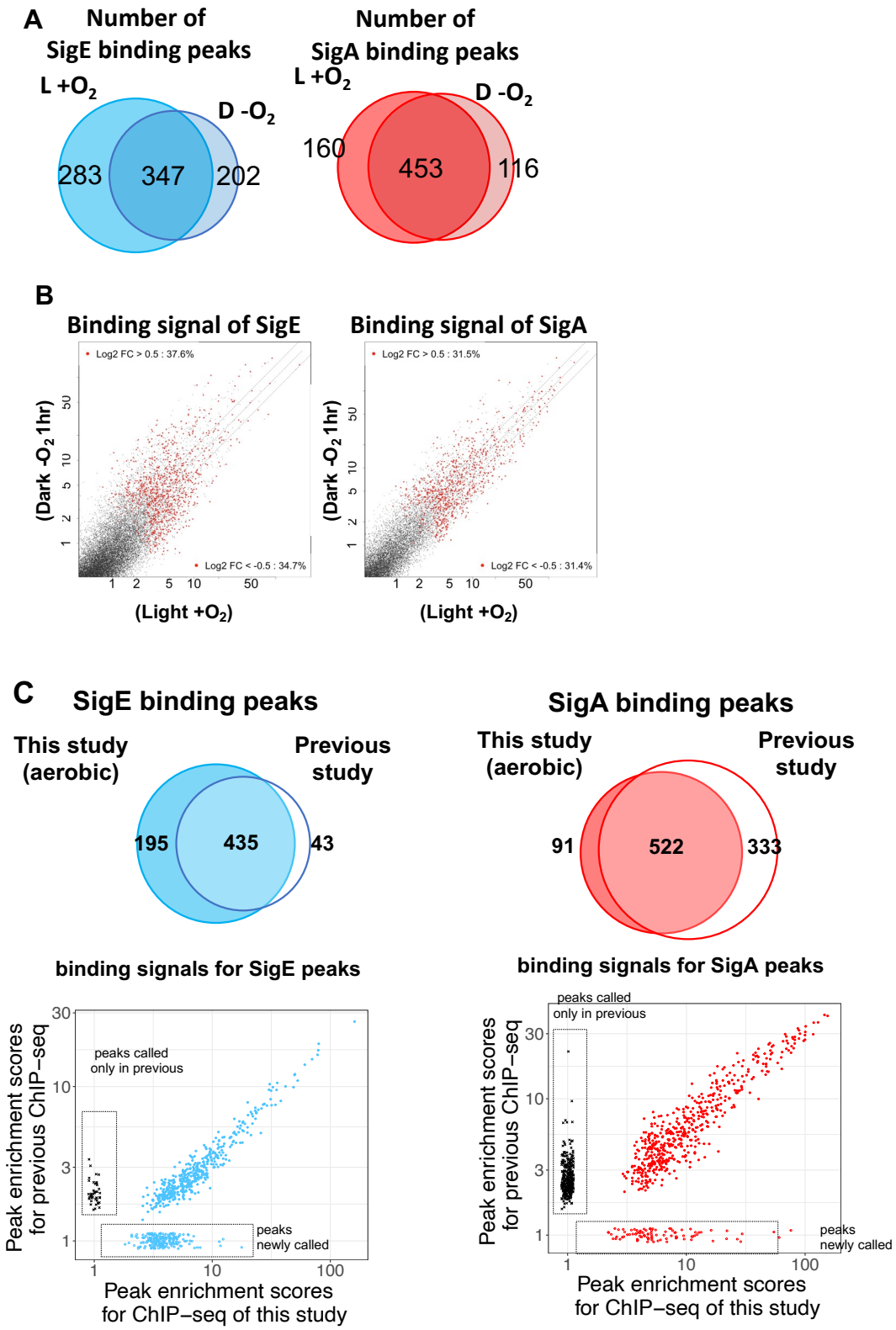

808

809 **Figure S7**

810 (A) Venn diagram showing the number of peaks of SigE (left) and SigA (right) in aerobic (L + O_2) and

811 dark microoxic (D − O_2) conditions. (B) Scatter plot showing changes in the binding signal of SigE and

812 SigA by 1 hour cultivation under microoxic conditions. The binding signal of each 100 bp window is

813 plotted. (C) Reproducibility of ChIP-seq data of SigA and SigE, compared with the previous study

814 (Kariyazono and Osanai 2022). (top) Venn diagrams show the overlapping of peaks called in this study

815 and the previous study. (bottom) Scatter plot comparing ChIP binding signals of SigA and SigE peaks

816 commonly called in present and previous studies. Plots boxed by dashed lines are peaks called only in the

817 present or previous study.

Figure S8

hox region (Figures 7A, 7B and 7C)

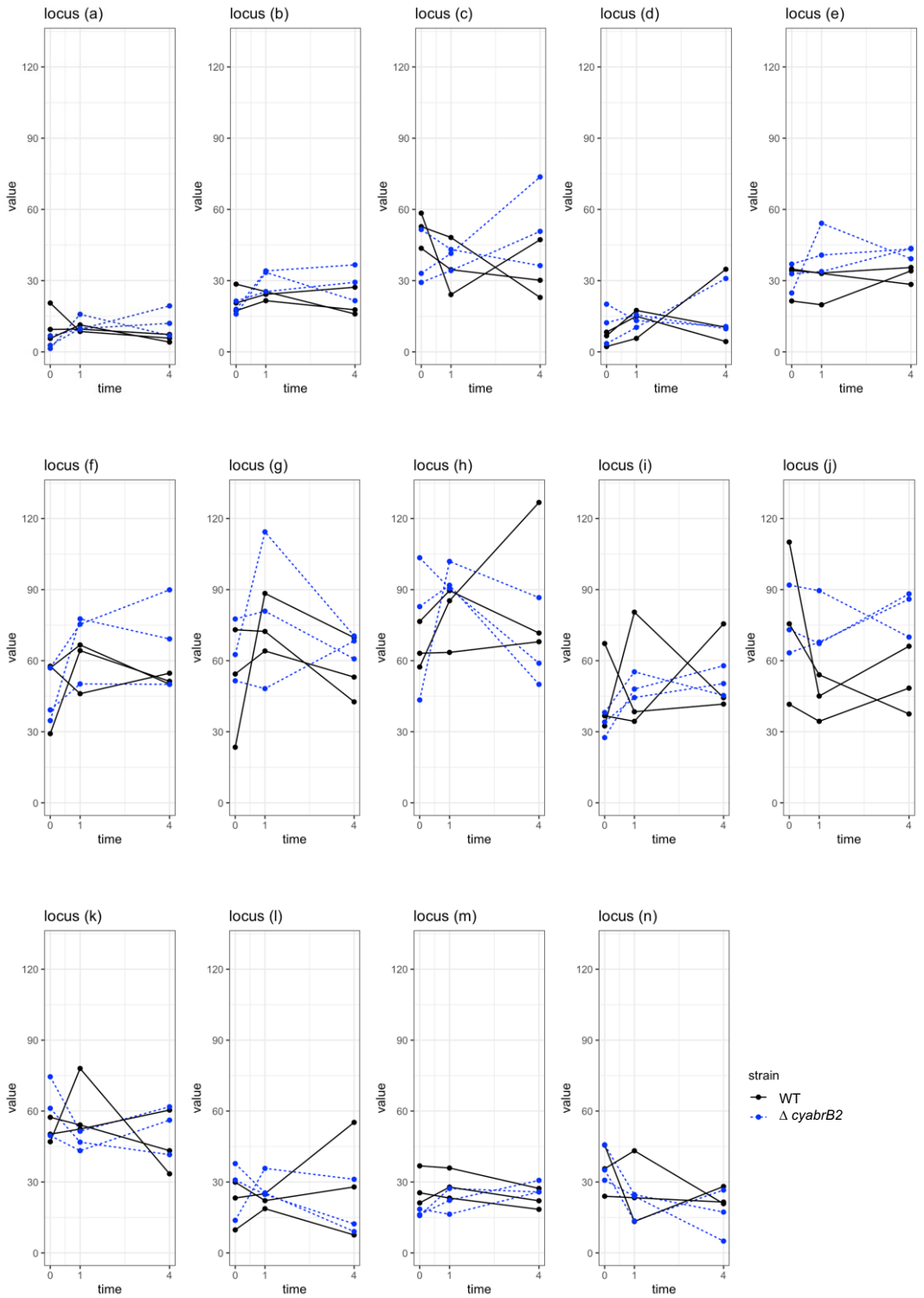

Figure S8 (continuing)

nifJ region (Figures 7D, 7E and 7F)

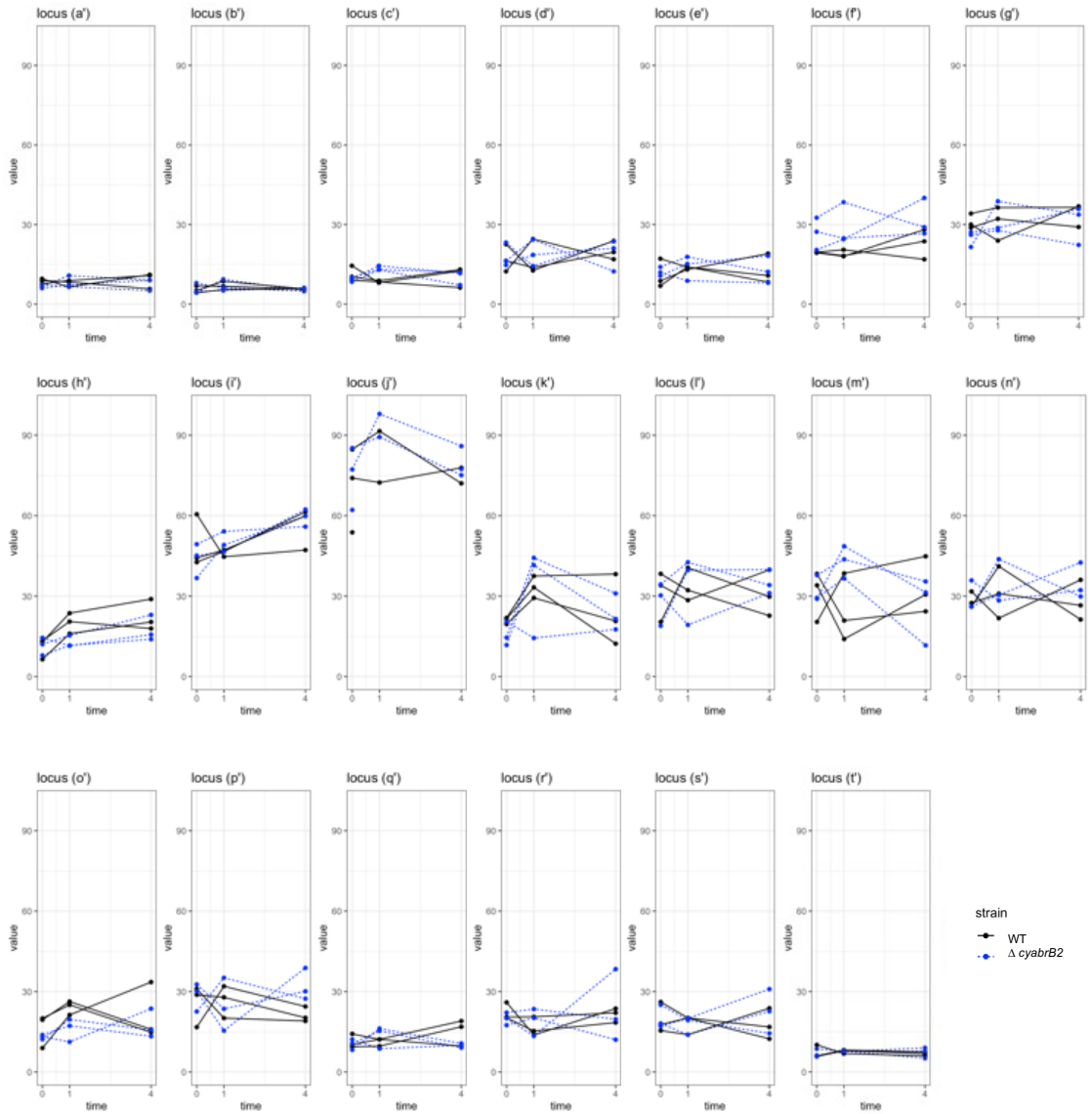

Figure S8 Dynamics of individual 3C scores

Re-plotting of Figure 5B and 5C with the x-axis showing time (0,1,4 hr in microoxic conditions) and the y-axis showing the interaction frequency. Plots from the individual samples are connected by solid (Wildtype) or dotty (Δ*cyabrb2*) lines.

Figure S9

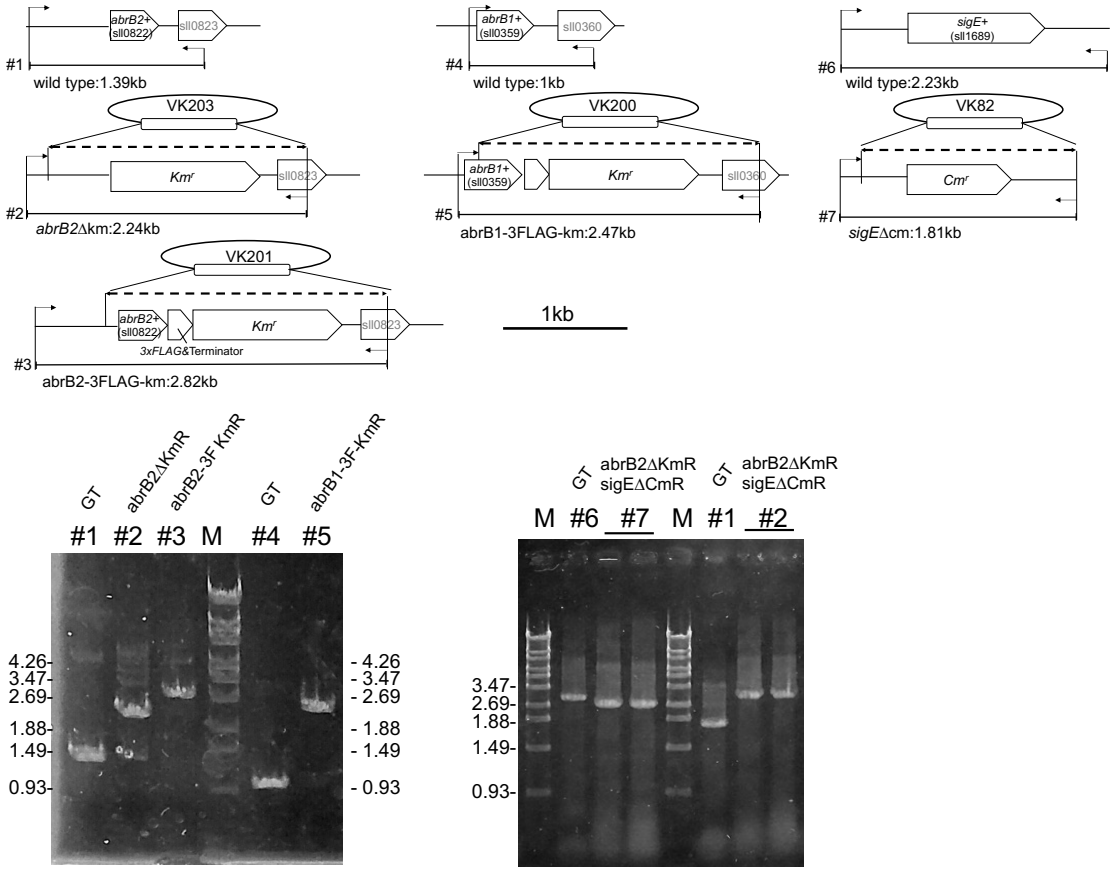

Figure S9

Confirmation of genomic deletion and the epitope tagging of *abrB2* (#1-#3), the epitope tagging of *abrB1* (#4 and #5), and deletion of *sigE* (#6 and #7). Dotty lines are homologous regions between plasmids and the genome. Arrows indicate the position of check primers.

Figure S10

A **3C primers for *hox* operon region**

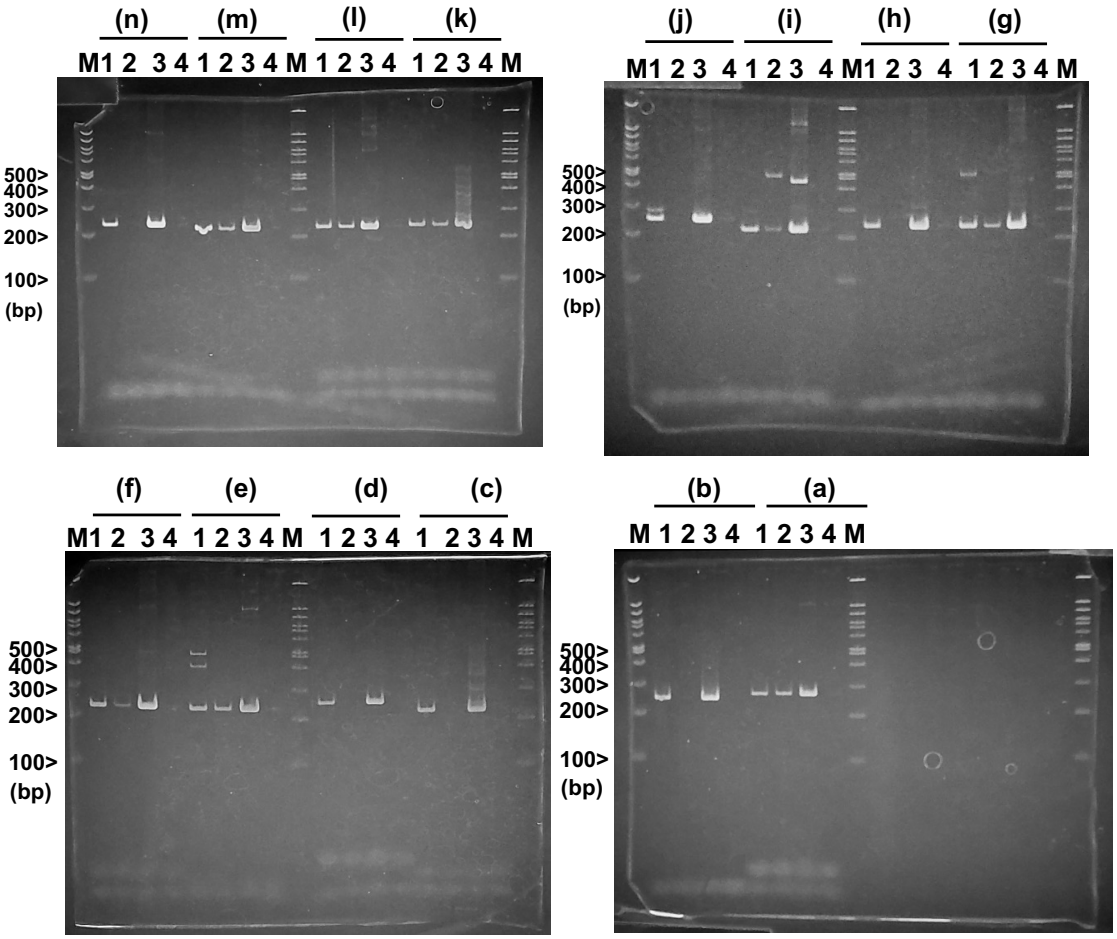

M:100bp ladder (DM2100 SMOBIO)
1 Calibration sample x500
2 Calibration sample x2500
3 3C sample x100
4 Unligated sample x100

GoTaq® Hot Start Program

95˚C 2min
95˚C 15sec | **x35**
60˚C 30sec |
4˚C Hold

830

Figure S10 (continuing)

B **3C primers for *nifJ* region**

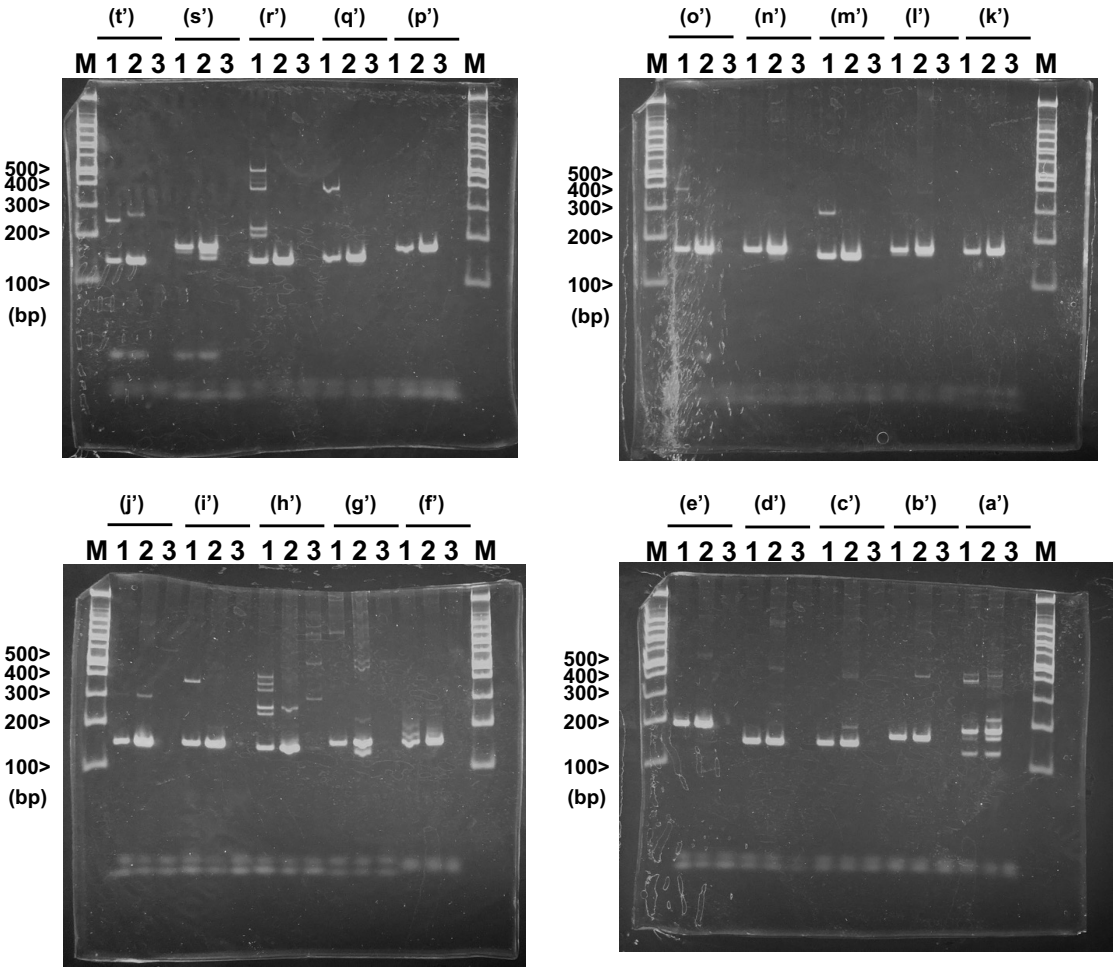

M:100bp ladder (DM2100 SMOBIO)
1 Calibration sample x1000
2 3C sample x100
3 Unligated sample x100

GoTaq® Hot Start Program

95˚C 2min
95˚C 15sec
60˚C 30sec
4˚C Hold

Figure S10 Validation of unidirectional primer sets for 3C assay

The validation of unidirectional primer sets for 3C assay is shown in Figure 7. The 3C sample in this assay is the mixture of all 3C samples assayed in Figure 7.

835 **Table S1 Fold changes of transcripts from *sigA, sigB, sigC, sigD, and sigE***

		0hr vs 1hr		1hr vs 4hr	
Sigma factor	**locus**	**Log2FC**	**FDR**	**Log2FC**	**FDR**
SigA	slr0653	-0.873248	0.00766486	-0.0013514	0.99797563
SigB	sll0306	1.38098826	8.42E-06	0.77453605	0.04057775
SigC	sll0184	2.97101055	1.75E-16	1.30743549	0.00067892
SigD	sll2012	0.4701823	0.1498473	-0.4522181	0.32402556
SigE	sll1689	-1.9111759	1.96E-11	-1.1223298	0.00633142

836 Data is extracted from Supplemental Table S7.

837

838 **Table S2 List of strains used in this study**

Strain ID	**Host strain**	**genotype**	**Reference**
GT			Williams, 1988
G50	GT	Δ*sigE::*KmR	T. Osanai, et al,2005
KR93	GT	SigA-8His-KmR	(Kariyazono and Osanai 2022)
KR94	GT	SigA-3FLAG-KmR	(Kariyazono and Osanai 2022)
KR340	GT	Δ*cyabrb2::*KmR	in this study
KR338	GT	cyAbrB(sll0359)-3xFLAG-KmR	in this study
KR339	GT	cyAbrB2(sll0822)-3xFLAG-KmR	in this study
KR359	KR340	Δ*cyabrB2::*KmR Δ*sigE::*CmR	in this study

839

840 **Table S3 plasmids used in this study**

Plasmid ID		**backbone**	
VK82	*sigE*ΔCmR	pTA2 (Toyobo)	transformation for KR359
VK200	AbrB1-3F-KmR	pTA2 (Toyobo)	transformation for KR338

VK201	AbrB2-3F-KmR	pTA2 (Toyobo)	transformation for KR339
VK203	*cyabrB2*ΔKmR	pTA2 (Toyobo)	transformation for KR340

841

842 **Table S4 oligonucleotides used in this study**

Oligonucleotides ID		**sequence**
qPCR_hoxF_F	Figure S2	GTCATCTGCAATGCTGACGAA
qPCR_hoxF_R	Figure S2	CCAACACACTGCGGTCCAT
qPCR_hoxH_F	Figure S2	TCCCGTTACCCGGATTGA
qPCR_hoxH_R	Figure S2	GCCCTGGTCGTTGAGGAAA
qPCR_nifJ_sll0741_F	Figure S2	GATTCGGGGCAAAGTTTACG
qPCR_nifJ_sll0741_R	Figure S2	TACCTGGATGGTGAACTTAG
qPCR_sll0744_F	Figure S2	GCAGCTTAAATGGTTCTACC
qPCR_sll0744_R	Figure S2	CCAAATCTGTGGGTACGTAG
qPCR_nrpB_F	Figure S2	AAAGGGTAAGGGTGCAAAGG
qPCR_nrpB_R	Figure S2	AATTCCTCAAGCGGTTCCAC
new_abrB_0822_del_chkF	Figure S9	AATCCTCCGCCAAACTTTG
abrB_0822_tag4	Figure S9	GACTGATGGTGAAAACTCC
abrB_0359_chkF	Figure S9	AGAGGGAAAAATTCCTCGGC
abrB_0359_tag4	Figure S9	TCGCCAGGGAAAGTAATTGG
SigE_whole_del_chkF	Figure S9	GGAACGCTTGGAATGGCAAC
sigE_tag4	Figure S9	TGAAGGGGGTAGATTTAAGCC
ChIP_slr2118_F1	Figure 5C #1	CATTTCAAGCGAGATAGCAG
ChIP_slr2118_R1	Figure 5C #2	TGGAAAGTGCCTGTTCAAAG
ChIP_ThoxH_F	Figure 5C #2	CATCACCGAGGGCATATCTAG
ChIP_ThoxH_R	Figure 5C #2	ACATAAGGCTATGGAAACC
ChIP_pHox_2F	Figure 5C #3	ACAGAGGATGGACAAATGTC
ChIP_pHox_2R	Figure 5C #3	TACCGCTTCGTCATTCTGCT
ChIP_pHox_up_2R	Figure 5C #4	TCGATTACTTCCCTTTAGTG
ChIP_pHox_up_2F	Figure 5C #4	CTTCGGCTCCATGTATTC
ChIP_sll0814_F	Figure 5C #5	GTTACTACCGCTATCTATCG

ChIP_sll0814_R	Figure 5C #5	ATGACGTAAACCGGCTCTGAC
3Chox_Hcommon	Figure 7 (hox region)	CGGTCCCTTTGGACGTAATC
3Chox_H01_pos_+1	Figure 7 (hox region)	GGGTTGGGCGCAACATTAAG
3Chox_H02_pos_+3	Figure 7 (hox region)	CAAAGCGATTTTGGCTGGTG
3Chox_H03_pos_+4	Figure 7 (hox region)	GATGTGGTGGAAGATACGGAC
3Chox_H04_pos_+5	Figure 7 (hox region)	GGAGCCACAGGGGAATTTAAC
3Chox_H05_pos_+6	Figure 7 (hox region)	GGTCAGATTTTATTGGTTGCATG G
3Chox_H06_pos_+7	Figure 7 (hox region)	TTGTCAATGTCAACCGCAAC
3Chox_H07_pos_+8	Figure 7 (hox region)	TTATTGCCCAATCTGGCGAC
3Chox_H08_pos_+11	Figure 7 (hox region)	AGGCAAGACAGATAAACCTTCTG
3Chox_H09_pos_-2	Figure 7 (hox region)	GGGGCATAGGGAGCAAACC
3Chox_H10_pos_-4	Figure 7 (hox region)	GGGGTAGTACCGGAAGTGG
3Chox_H11_pos_-6	Figure 7 (hox region)	TTGGGCTGATTCTTGCAATTC
3Chox_H12_pos_-11	Figure 7 (hox region)	AGCTTTTGTCTAACACCGTATCG
3Chox_H13_pos_-13	Figure 7 (hox region)	AAGCCATCCTTCAAAACCCG
3Chox_H14_pos_-17	Figure 7 (hox region)	GCCCCATCGGTGAGAAAAAG
qPCR_hoxF_F	Figure 7 (hox internal control)	GTCATCTGCAATGCTGACGAA
qPCR_hoxF_R	Figure 7 (hox internal control)	CCAACACACTGCGGTCCAT
3CnifJ_Hcommon	Figure 7 (nifJ region)	ATTCTTTTCGCCAGTTTCTCCAC
3CnifJ_H01_pos-16	Figure 7 (nifJ region)	CATGCTGTTCTGTGCCCATC
3CnifJ_H02_pos-14	Figure 7 (nifJ region)	TCAGTGATATTTTGACCGCTGG
3CnifJ_H03_pos-13	Figure 7 (nifJ region)	AAAACCCCTGCCAACAAGAC
3CnifJ_H04_pos-12	Figure 7 (nifJ region)	CTCCCCACAATAAAGGGCTG
3CnifJ_H05_pos-10	Figure 7 (nifJ region)	TCATAGAAGCGGCGGATACC
3CnifJ_H06_pos-8	Figure 7 (nifJ region)	AGATAACGCCCCGGAACC
3CnifJ_H07_pos-7	Figure 7 (nifJ region)	GTATGGGTCGCCAAAGTACG
3CnifJ_H08_pos-6	Figure 7 (nifJ region)	AGGGATGGGGATCTTTGCTG
3CnifJ_H09_pos-4	Figure 7 (nifJ region)	TTATTGCTTTCACCCCGGC
3CnifJ_H10_pos-3	Figure 7 (nifJ region)	GCCCTAGGCCAAAGAATACC
3CnifJ_H11_pos-1	Figure 7 (nifJ region)	CCAGCCAGGGAGATGACC
3CnifJ_H12_pos+1	Figure 7 (nifJ region)	GCCATTGGGGGTTTATTGGC
3CnifJ_H13_pos+2	Figure 7 (nifJ region)	GTAAACAGATAGGTGGTGCGG

3CnifJ_H14_pos+6	Figure 7 (nifJ region)	TACAAAGCCAGGTAAGCGTC
3CnifJ_H16_pos+8	Figure 7 (nifJ region)	TCTGACCTATTGCCCTGACC
3CnifJ_H17_pos+9	Figure 7 (nifJ region)	CTGTTGTCATTGCTTGCTCC
3CnifJ_H18_pos+11	Figure 7 (nifJ region)	TGTAGCCAGTGAAGGGGAAG
3CnifJ_H19_pos+14	Figure 7 (nifJ region)	TCCCGGTATTAATGGCATTGG
3CnifJ_H20_pos+15	Figure 7 (nifJ region)	GTTGTGTGATTCCCCAAGCC
3CnifJ_H22_pos+17	Figure 7 (nifJ region)	CTTATTTTGTACCCGGCACCC